INITIAL INVESTIGATION OF AN INDUCTIVE COIL TECHNIQUE FOR THE DETERMINATION OF THE EQUIVALENT ELECTRICAL CONDUCTIVITY OF A TWO PHASE LIQUID METAL FLOW

Barry T. Lubin

Massachusetts Institute of Technology
Cambridge, Massachusetts

September 1965

INITIAL INVESTIGATION OF AN INDUCTIVE COIL TECHNIQUE FOR THE DETERMINATION OF THE EQUIVALENT ELECTRICAL CONDUCTIVITY OF A TWO PHASE LIQUID METAL FLOW

by

BARRY T. LUBIN

B. S. E., University of Connecticut
1959

M. Eng., Yale University
1960

Submitted in Partial Fulfillment of the
Requirements for the Degree of
Mechanical Engineer

at

Massachusetts Institute of Technology
September 1965

Signature of Author Barry T. Lubin
Department of Mechanical Engineering
August 23, 1965

Certified by George A. Brown
Thesis Supervisor

Accepted by _____
Chairman, Departmental Committee on
Graduate Students

ABSTRACT

INITIAL INVESTIGATION OF AN INDUCTIVE COIL TECHNIQUE FOR THE DETERMINATION OF THE EQUIVALENT ELECTRICAL CONDUCTIVITY OF A TWO PHASE LIQUID METAL FLOW

Submitted to the Department of Mechanical Engineering on August 23, 1965, in Partial Fulfillment of the Requirement for the Degree of Mechanical Engineer.

An inductive measuring technique has been used in conjunction with a nonlinear, twin T type of bridge in an effort to correlate bridge output with the coil core electrical conductivity. This is envisioned as being the initial step in designing an instrument capable of detecting changes in electrical conductivity of a two phase liquid metal flow, as applied to an MHD power generation cycle. Definite measurements were achieved, but poor agreement exists between the present theory and the data obtained. The data was not definitive enough to establish any reliable calibration. Even though no two phase flow measurements were attempted, the instrument did show a potential of being used to determine the relative electrical conductivity between highly conducting materials.

Thesis Supervisor: George A. Brown

Title: Associate Professor of Mechanical Engineering

Acknowledgments

There are basically two forms of outside influence received by an author in a project of this degree; moral encouragement and technical advice. Both were freely given by my advisor Professor George Brown plus one more influence of not the usual sort; sympathy. Sympathy for the mechanical engineer, like he and I, trying to in some small way to master the more abstract world of the electrical engineer. To this end I should also like to acknowledge the help of Professor William D. Jackson of the Electrical Engineering Department.

Acknowledgement is also due to the M.I.T. Computation Center where the theoretical calculations were carried out in part, and both the U.S. Air Force (ASD), Wright Field (Contract AF 33(615) - 1083) and the Joint Services Electronic Program (Contract DA 36-039-AMC-03200(E)) which provided the financial support for this project.

Table of Contents

List of Figures

List of Tables

Nomenclature

σ	Electrical conductivity (MHO/meter)
$\bar{\sigma}$	Equivalent electrical conductivity
α	Volume void fraction
$K \equiv \frac{\sigma_1}{\sigma_2}$	1 void material 2 major material
ρ	Density
$\dot{Q}$	Volume flow
A	Area
τ	Surface tension
g	32.2 ft/sec^2
μ_o	Permiability of air (1.25×10^{-6} Henry/meter)
ω	Frequency (rad/sec)
f	Frequency (cps)
r_c	Core radius (m)
r	Radius (m)
δ	Skin Depth (m)
ℓ	Coil length (m)
N	Winding turns
i_o, i_z, i_r	Unit direction vectors
$\underline{\underline{I}}$	Current (amps)
$\underline{\underline{E}}$	Electric field (volt/m)
$\underline{\underline{H}}$	Magnetic field (amp-turn/m)

$\underline{\bar{J}}$ Current density (amp/m^2)

ϕ Potential (volts)

r, θ, z Cylindrical coordinates

L Inductance (Henries)

V Voltage (volts)

$\underline{\bar{S}}$ Poynting vector

$\langle P \rangle$ Time average real power (Watts)

$\langle Q \rangle$ Time average reactive power (Watts)

Ω Coil winding resistance (Ohms)

Q Coil energy storage / Coil Ohmic dissipation Factor

$j \equiv \sqrt{-1}$

Z Impedance (Ohms)

η Core radius to skin depth ratio

R Total resistance of bridge

T Period = $1/f$

r Resistance sum

k Bridge parameter

S Sensitivity $(\frac{volts}{Ohm})$ or $(\frac{amp}{Ohm})$

$f( )$ Function of

C Bridge correction factor

E Bridge voltage { 0 output; 1 input }

$\Delta E \equiv (E_o)$ metal $- (E_o)$ air

∇ Del Operator (Cylindrical Coordinates) $\equiv \bar{u}_r \frac{\partial}{\partial r} + \bar{u}_\theta \frac{1}{r} \frac{\partial}{\partial \theta} + \bar{u}_z \frac{\partial}{\partial z}$

1.0 Introduction

With the recent interest in space power systems to produce power in the MW range, the use of MHD power generation for this application has taken a position of increased importance. References 1-4 contain analyses of various power cycle arrangements, utilizing both gas and liquid phases in some portion of a liquid metal MHD cycle. In all of these configurations, it is of prime importance that the gaseous and liquid phases are separated as completely as possible before entering the generator, since the electrical conductivity (σ) of the pure liquid is reduced by the presence of the gas. Thus it is important to have a knowledge of the relationship between the percentage of vapor and the equivalent electrical conductivity ($\bar{\sigma}$) of the mixture as seen by the generator. This report covers work carried out in the initial phase of both analytically and experimentally determining a relationship between the equivalent electrical conductivity and the vapor void fraction.

The departure point for this study was a review of the various derivations for equivalent electrical conductivity of a heterogeneous media, all of which can be traced back to the classical work of J. C. Maxwell (5). [+] In order to verify

---

[+] Numbers in parentheses refer to references in the bibliography.

these relationships, an inductive coil measuring technique was selected to be developed into an instrument capable of detecting small changes in electrical conductivity. A simplified analysis was derived for the equivalent electrical impedance for a coil of cylindrical geometry, having a core of a nonmagnetic, but electrically conducting material. With the establishment of the design parameters for the coil, it was then possible to construct a series of experiments to detect and correlate changes in coil parameters with electrical conductivity changes. During this phase of the work such changes were introduced by using solid cores of different electrical conductivity instead of having a true flow situation.

The coils designed were used in conjunction with two types of comparative null balance bridges: the common Maxwell bridge and a nonlinear "Twin T" bridge. In order to obtain the necessary sensitivity, the T bridge was found more suitable, and a series of experiments was carried out with this type of bridge.

Recordable changes in bridge output were detectable with this bridge arrangement, and an attempt was made to correlate experimental data and analytical predictions. The results showed qualitative agreement, but poor quantitative correlation. Both inadequate equipment sensitivity and theory

inadequacies were felt to be the cause of the discrepancy.

In conclusion, attempt was made to explain these differences in order to improve the agreement between the present measurement technique and theory.

2.0 Equivalent Electrical Conductivity

The classical derivation of the equivalent electrical conductivity of a heterogeneous mixture was first carried out by Maxwell (5). Using the assumption of a normally homogeneous media interdispersed with a material of a different electrical conductivity, Maxwell replaced this material with an "equivalent" material, equivalent in the sense that the same electric field is maintained throughout both materials. Thus, an equivalent electrical conductivity ($\bar{\sigma}$) could be defined. Assuming that the dispersed phase is of spherical particles and is sufficiently dilute so that no point contact exists amongst these particles, Maxwell was able to express the electric field in terms of spherical harmonics (Le Condre polynomials) in the steady state. By applying the electromagnetic boundary conditions between the two phases, as well as considering the finite character of the fields, the constants of the field equations were solved for. After replacing the heterogeneous mixture by one of conductivity $\bar{\sigma}$, and a volume α times the original homogeneous phase volume, $\bar{\sigma}$ was solved for as a function of α. The resulting expression due to Maxwell is

$$\frac{\bar{\sigma}}{\sigma_2} = \frac{2\alpha(\sigma_1-\sigma_2)-(\sigma_1+2\sigma_2)}{\alpha(\sigma_1-\sigma_2)-(\sigma_1+2\sigma_2)}$$

where 2 is the normally homogeneous phase and 1 is the dispersed phase. (See Table I).

A group of Russian works (references 8, 10, 9) extend the basic Maxwell work to a more generalized form. Korneenko (9), by using Gauss's theorem, related the volume characteristic of any shaped inclusion to the boundary conditions and showed how the average conductivity value of the media could be derived in a more general manner. Pliat (10) presents an equation derived for the thermal conductivity of a "statistical" mechanical mixture of solid materials. With the analogy between heat flow and electric field theory, this should also apply to the present case.

Lord Rayleigh, by neglecting Maxwell's assumption that the inclusions do not effect the field in the homogeneous media, extended Maxwell's equation to a slightly more general form. Meredith (6) noted the incorrectness of both Maxwell and Rayleigh if the spherical inclusions are in point contact. He derived an even more general equation by extending the electric field equations to include more terms of the Le Gendre polynomials accounting for point contact in the limit. Referring to Table I, a summary of these equations is presented. Figure 1 shows the comparison of the Maxwell, Rayleigh, and Meredith equations for a limiting case of

Table I Comparison of Theoretical Equations for Equivalent Electrical Conductivity of a Two Phase Mixture

where $K = \frac{\sigma_1}{\sigma_2}$ $\quad \alpha = \frac{V_1}{V_2}$, volume void fraction

Maxwell:

$$\frac{\bar{\sigma}}{\sigma_2} = \frac{2\alpha(1-K) - (K+2)}{\alpha(K-1) - (K+2)}$$

Rayleigh:

$$\frac{\bar{\sigma}}{\sigma_2} = \frac{\left(\frac{2+K}{1-K}\right) - 2\alpha - .525\left(\frac{3-3K}{4+3K}\right)\alpha^{10/3}}{\left(\frac{2+K}{1-K}\right) + \alpha - .525\left(\frac{3-3K}{4+5K}\right)\alpha^{10/3}}$$

Meredith:

$$\frac{\bar{\sigma}}{\sigma_2} = \frac{\left(\frac{2+K}{1-K}\right) - 2\alpha + .409\left(\frac{5+3K}{4+3K}\right)\alpha^{7/3} - 2.133\left(\frac{3-3K}{4+3K}\right)\alpha^{10/3}}{\left(\frac{2+K}{1-K}\right) + \alpha + .409\left(\frac{5+3K}{4+3K}\right)\alpha^{7/3} - .906\left(\frac{3-3K}{4+3K}\right)\alpha^{10/3}}$$

Fricke:

$$\frac{\left(\frac{\bar{\sigma}}{\sigma_2} - 1\right)}{\left(\frac{\bar{\sigma}}{\sigma_2} + \chi\right)} = \frac{\alpha(K-1)}{(K+\chi)}$$

$\chi = f(t/b, K)$

$\chi = 2$ for spheres

Pliat:

$$\frac{\bar{\sigma}}{\sigma_2} = \frac{(3\alpha-1)K + (2-3\alpha)}{4} + \sqrt{\left[\frac{(3\alpha-1)K + (2-3\alpha)}{4}\right]^2 + K}$$

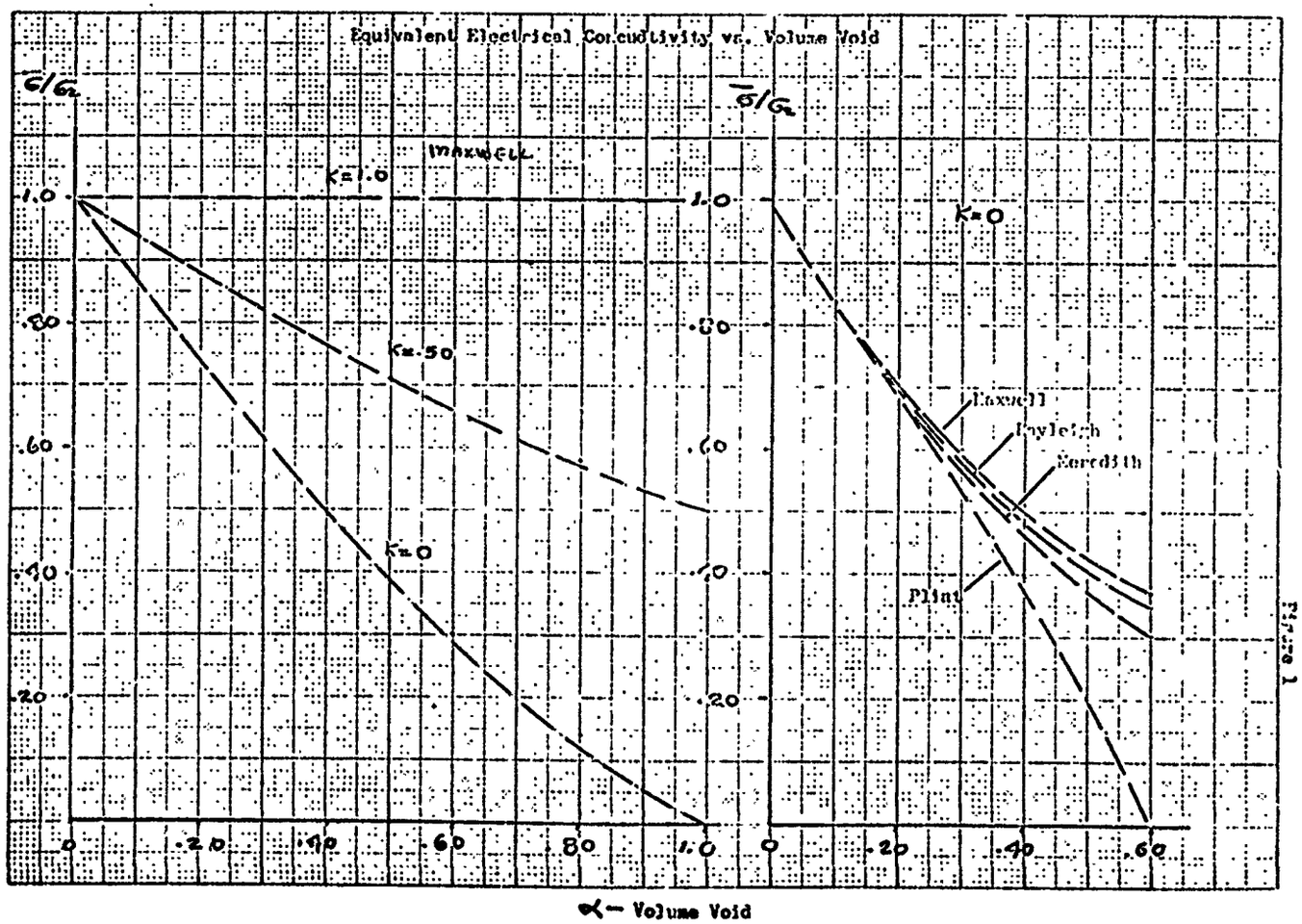

Figure 1

the dispersed phase being of zero conductivity (i.e. $\sigma_2 << \sigma_1$). It can be noted that in this case all three forms of the equation reduce to Maxwell's equation plus correction terms.

$$\frac{\bar{\sigma}}{\sigma_2} = \frac{(1-\alpha)}{(1+\alpha/2)} + \text{---} \quad \text{correction terms}$$

Figure 1 is a representation of Maxwell's result as a function of void fraction and the dispersed phase conductivity.

To complete the discussion of the theoretical work on electrical conductivity, Reference 7 by Fricke contains a derivation for other than a purely spherical inclusion. Fricke's primary interest was conductivity of blood. His derivation was generalized for ellipsoids of revolution, with his result expressed as a function of the ellipsoid aspect ratio, (a/b), and the $\frac{\sigma_1}{\sigma_2}$ ratio.

The main conclusion of this work as applied to the problem at hand is that there exist only negligible differences in $\bar{\sigma}$ for a/b = 1.0 (sphere) as compared to $\bar{\sigma}$ for changes in a/b as large as 100 per cent.

2.1 Nature of the Two Phase Flow

Some brief comments will be presented as to the nature of two phase flow, so that the preceding remarks on the

Table II Theoretical Equivalent Electrical Conductivity for Gas Voids

Maxwell:

$$\frac{\bar{\sigma}}{\sigma_2} \approx \frac{(1-\alpha)}{(1+\alpha/2)}$$

Meredith:

$$\frac{\bar{\sigma}}{\sigma_2} = \frac{2-2\alpha+.613\alpha^{7/3}-1.60\alpha^{10/3}}{2+\alpha-.613\alpha^{7/3}-.650\alpha^{10/3}}$$

Fricke:

$$\frac{\bar{\sigma}}{\sigma_2} = \frac{(1-\alpha)}{(1+\alpha/2)}$$

Fliat:

$$\frac{\bar{\sigma}}{\sigma_2} = (1-3/2\alpha)$$

applicability of the $\bar{\sigma}$ expressions can be put into a better perspective.

One of the main objects of the MHD power cycle is to maximize power. To have the maximum σ of the working fluid, it is desirable that the percentage of vapor be as small as possible. Thus it would be expected that, discounting the effect of the magnetic field on the vapor, the flow would most likely be of a bubbly nature--consisting of small vapor voids dispersed fairly evenly throughout the flow field. References 20 and 22 review the nature of the relationship between void fraction (volume per cent of vapor) and the flow velocities in the bubbly flow regime. This expression is of the form

$$\left(\frac{\dot{Q}_{gas}}{A_{flow}}\right) = \text{constant}\left[\frac{\tau_g(\rho_l - \rho_g)}{\rho_l^2}\right]^m (1+\alpha)(\alpha^n)$$

A review of the derivation and determination of the constants is not required in this work. The important note is that this equation should correlate for bubbly flow in the range of interest of this present MHD generator concept. Thus, it can be assumed that Maxwell's equation or a modification thereof should be adequate to describe $\bar{\sigma}$ for this type of flow.

3.0 Measurement of the Equivalent Conductivity

With an initial foundation for the analytical relationship between $\bar{\sigma}$ and α established, experimental verification is required. This requirement is most logically fulfilled by a series of experiments starting with determining changes of electrical conductivity without the complication of two phase flow, then progressing to a stagnant flow with a vapor phase introduced into the fluid, and finally to as complete an MHD flow situation as possible.

The major problem is detecting the changes in σ. An inductive coil method, the coil being of cylindrical geometry, not only presents a good flow geometry for all these experiments, but also permits the flow to be undisturbed while the coil "sees" an equivalent conductivity of the flow. The induction coil method is based on the principle that by applying a time varying current to the coil windings, a magnetic field is established within the core space. This time varying magnetic field induces an electric field in the core. With a core of zero conductivity and resistanceless windings, no real power is taken by the coil and core. But if the core is of a finite conductivity, some real power is absorbed as Joulean heat loss, thus changing the equivalent electrical impedance of the coil.

By varying this conductivity, the change of impedance can be determined as a function of conductivity. An operational upper limit is established by the skin depth phenomena; for at "infinite" conductivity no field can exist in the core, and thus no losses will be induced. A brief review of the coil parameters will clarify this point further.

This measurement technique is by no means new, references 14-17 contain results of using this basic technique in measuring conductivity of gases. However, a limitation that is not restrictive in the construction of these experiments referred to is the limiting restriction in the present experiment; that being the assumption of negligible skin effect, or;

$$\sigma << 2\left(\mu_0 \omega r_c^2\right)^{-1}$$

Since references 14-17 are concerned primarily with the determination of gas conductivity in the order of $10^0 - 10^3$ MHO/meter, for reasonable coil sizes, the frequency of operation is in the megacycle range. As will be subsequently derived, the induced electric field is proportional to ω^2. Thus, the increased sensitivity of these experimental setups is due to the higher frequency range as compared to the present work in which σ is about $10^6 - 10^8$ MHO/meter and the skin depth limits to the $10^2 - 10^3$ cycle range. Figure 2 shows the relationship for skin depth defined as,

$$\delta = \left[\frac{\sigma}{2\mu_0 \omega}\right]^{1/2}$$

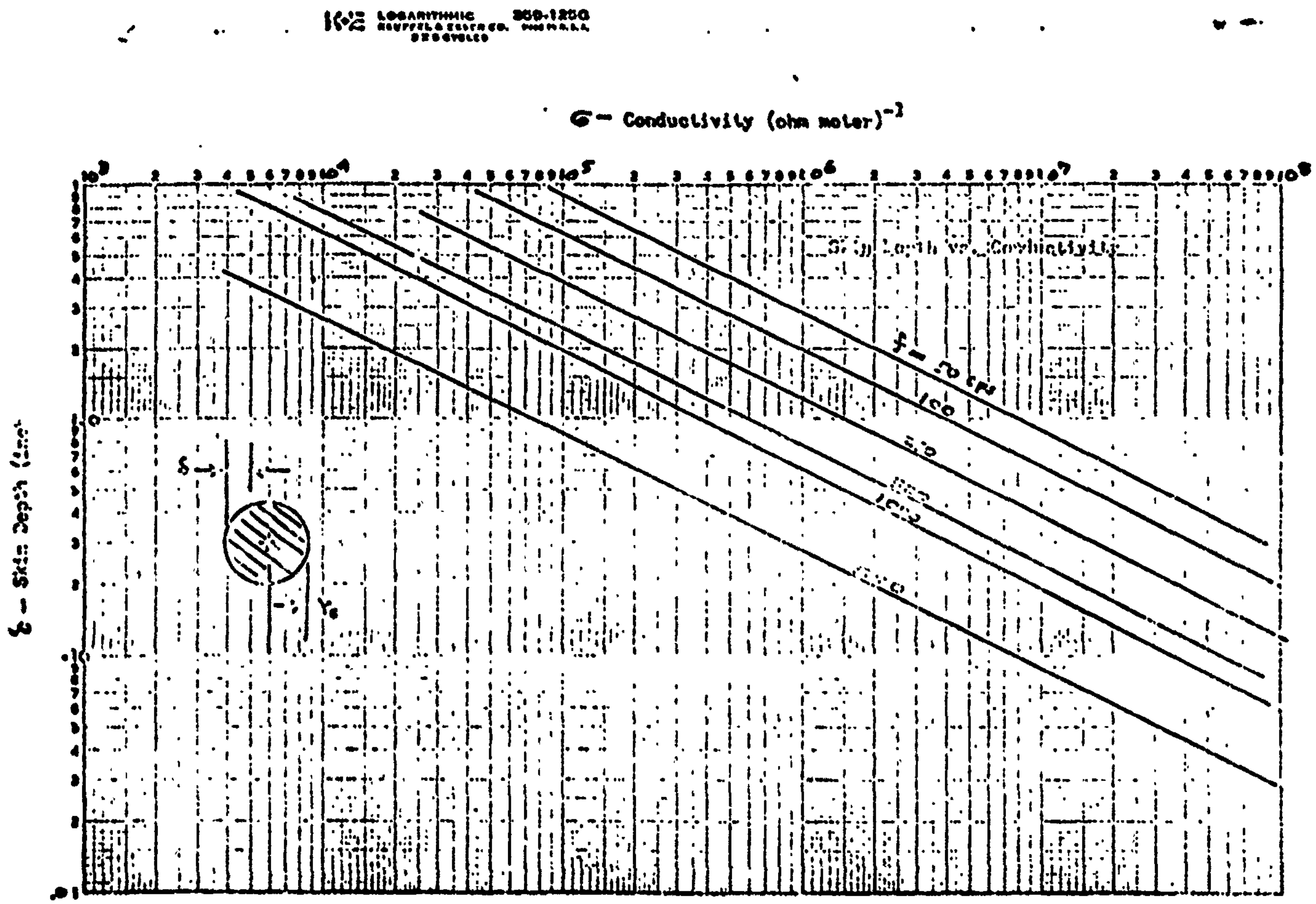
K&E LOGARITHMIC 359-120G
σ – Conductivity (ohm meter)$^{-1}$
δ – Skin Depth
Skin Depth vs. Conductivity
f = 50 cps
100
δ
r_s

Figure 2

3.1 Changes in Coil Parameters due to Changes in Conductivity

The item of major interest from the derivation of the field equations for a cylindrical coil (Appendix A), is the magnitude of the change of coil impedance due to changes in σ.

The impedance is given by,

$$\frac{Z_2}{\Omega} = \left[Q^2 + 1 + \frac{Q q_1^2}{4} \left(\frac{Q q_1^2}{4} + 2 \right) \right]^{1/2}$$

where $$Q \equiv \frac{\omega L}{\Omega} \quad , \quad q_1 \equiv \frac{r_c}{\delta}$$

The change Z_2/Ω with the percentage change in σ can be derived by partial differentiation as,

$$\frac{\partial (Z_2/\Omega)}{\partial \sigma/\sigma} = \frac{\frac{Q q_1^2}{4} \left(\frac{Q q_1^2}{4} + 1 \right)}{\left[Q^2 + 1 + \frac{Q q_1^2}{4} \left(\frac{Q q_1^2}{4} + 2 \right) \right]^{1/2}}$$

The total core plus coil resistance is given by,

$$R_2 = \Omega \left[1 + \frac{Q q_1^2}{4} \right]$$

The percentage change in resistance with change in conductivity is,

$$\frac{\partial (R_2/\Omega)}{\partial \sigma/\sigma} = \frac{Q q_1^2}{4}$$

Since the analysis was carried out for the assumption of $r_c \leq \delta$, q_1 is limited to a maximum value of 1.0.

Figures 3,4, and 5 present the variation of the change in Z_o/Ω and R_L/Ω as a function of ζ, for values of Q. Since to obtain the greatest change in R or Z_o the operational frequency $\omega = 2\pi f$ would be such that $\delta = r_o$, this $\zeta = 1.0$ would be the limiting value. From these plots, it is evident that as large a value of Q as possible is necessary for adequate detection of any change in R_L or Z_o. Q is limited by practical coil size, and thus to a maximum value of about 100. For a coil of Q = 100

$$\Delta\left(\frac{R_L}{\Omega}\right) \cong 25 \frac{\Delta\sigma}{\sigma}$$

For a liquid metal core of $\sigma \cong 10^6$ MHO/meter the change in R_L due to void fraction variations that must be detected is of the order of magnitude of $(1/10^4)$, while for an air core being replaced by a copper core, the theory predicts changes on the order of 25 times the coil resistance. Yet, the change from a copper core to aluminum core (10^8 to 10^7 MHO/meter) is of the same order of magnitude change as that due to the possible void fraction variations.

It is clear that the objective of this experiment is to design a coil of as high a Q as is practically possible, and to incorporate this coil in a device capable of detecting changes in the equivalent coil resistance of $1/10^4$ parts. This suggests some form of null balance or bridge circuit. An

Figure 3

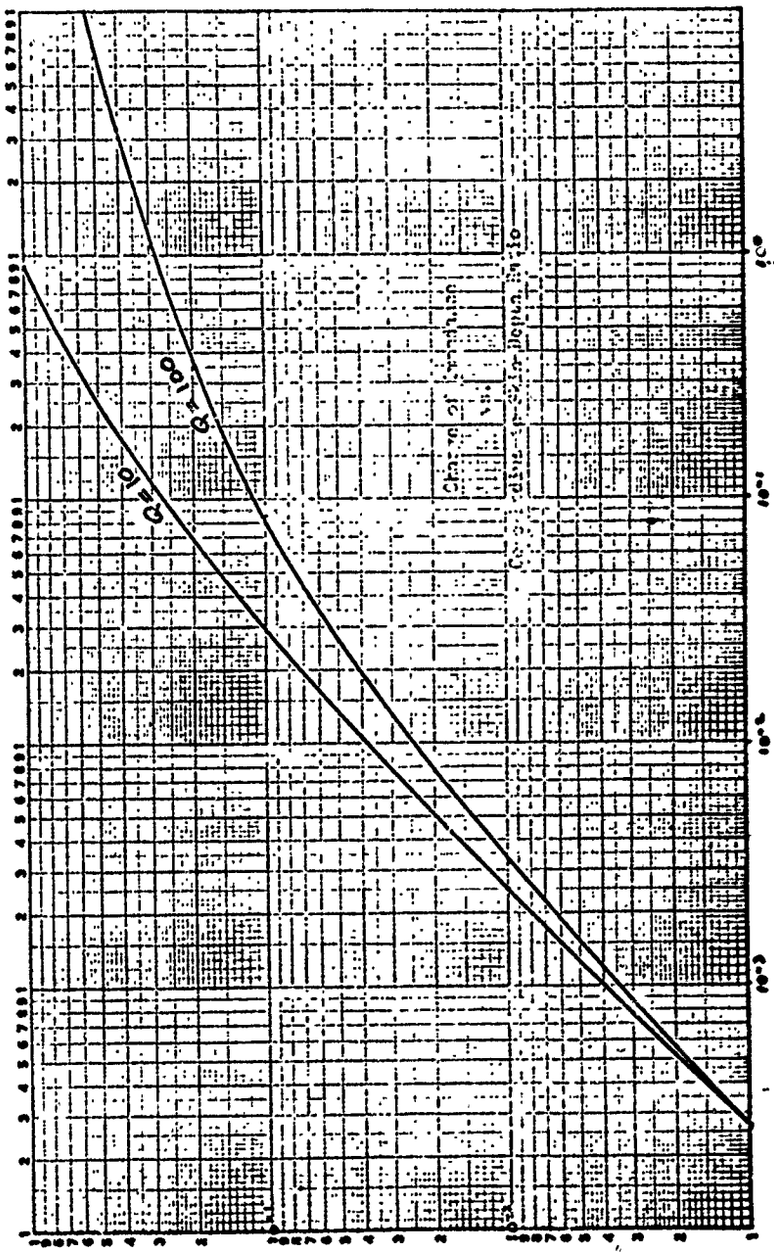

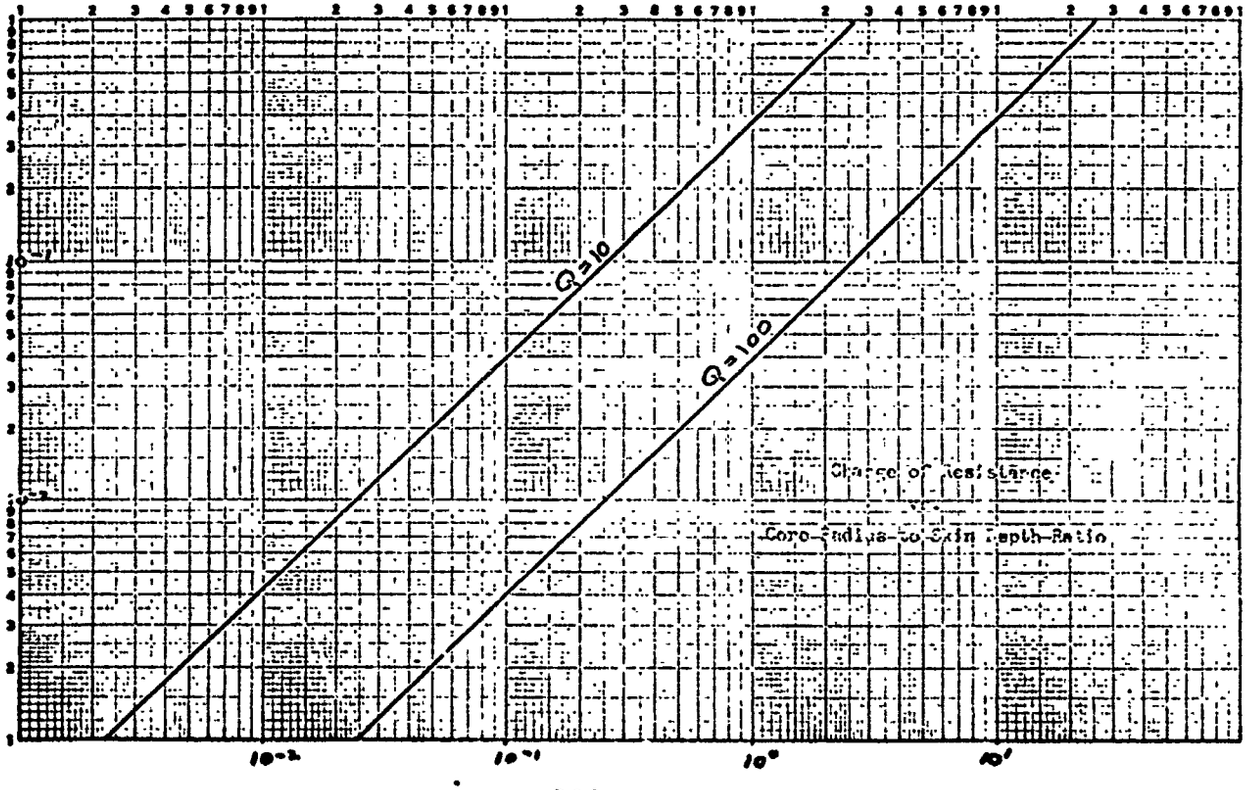

$\frac{\partial R/R}{\partial \sigma/\sigma}$

Figure 4

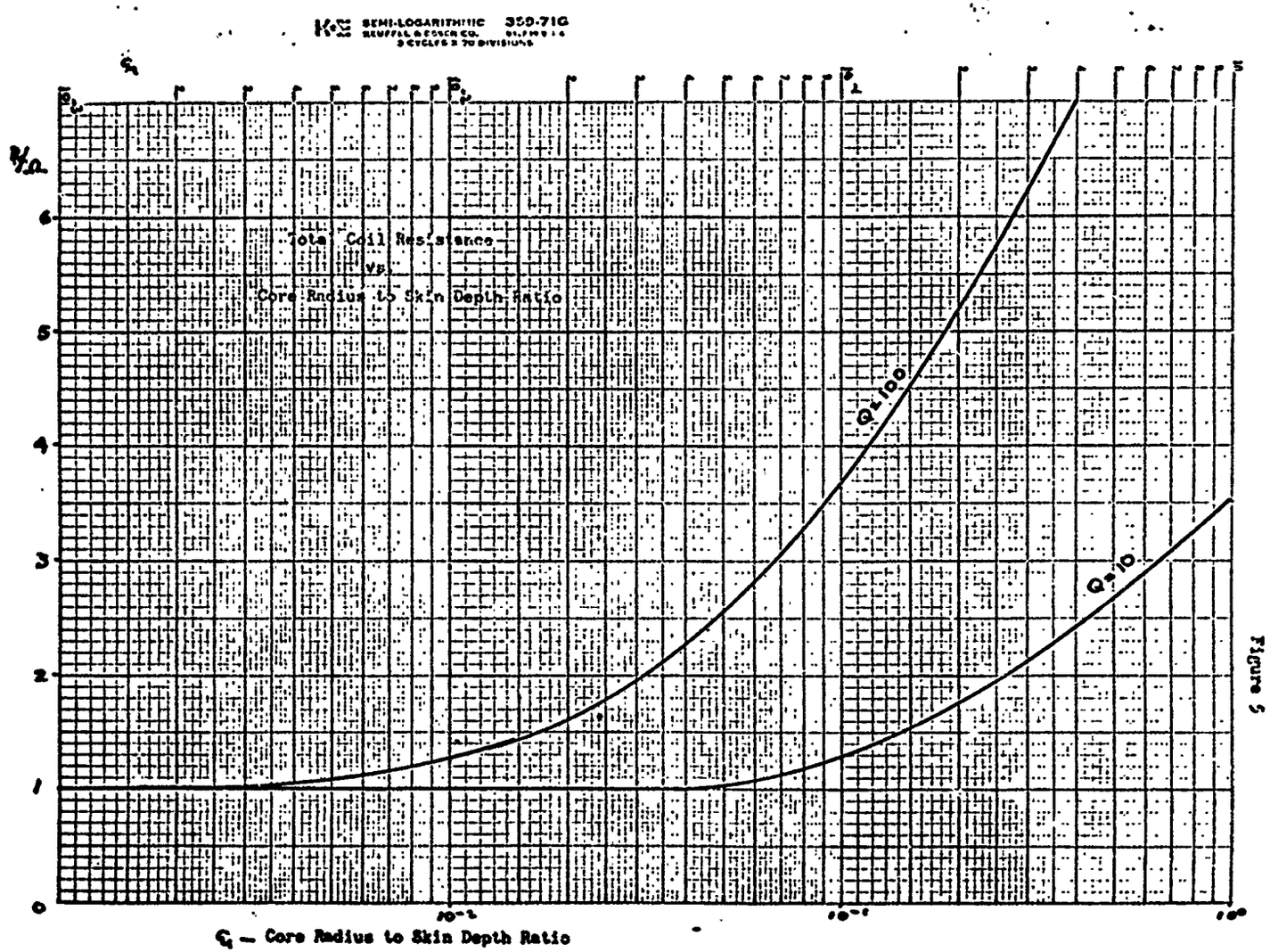

ζ_1 — Core Radius to Skin Depth Ratio

Figure 5

ordinary Wheatstone bridge circuit is shown in the work of Reference 15 on conductivity determination in hypersonic wakes. Yet, as previously mentioned, the frequency limitation due to skin depth will limit the range of ordinary bridge operation for the present application.

3.2 Skin Depth Limitations

Before a review of the experimental measurements is undertaken, some clarification on skin depth limitation is necessary. By definition, the skin depth, δ , is that depth at which the electric field in a conductor of finite conductivity has decayed to 1/e of its value at the surface. For sinusoidal steady state, δ is given by

$$\delta = \left(2/\omega\mu_0\sigma\right)^{1/2}$$

Thus, for $\sigma \to 0$, $\delta \to \infty$ and the field completely penetrates the conductor. For $\delta = r_c$, ω can be quite high. But, as $\sigma \to \infty$, $\delta \to 0$ and the electric and magnetic fields become excluded from the core region. Note that the fields in the region around the outside of the coil still exist. Since L is a measure of the magnetic field storage, below the skin depth limit, L is constant and greater than the value when the skin depth is exceeded. For a fixed r_c and σ , as ω is increased past the limit of $\delta = r_c$, L will decrease.

Therefore, changes in the coil impedance are no longer due to changes in R alone, but also to changes in L. For a two phase flow, the skin depth is a very uncertain quantity, being dependent on the flow pattern as well as $\bar{\sigma}$. In order for the measurements to be independent of changes in L, the range of frequency operation of the detection device is restricted to values below which the skin depth is exceeded.

4.0 Experimental Measurements

Experimental verification of the theory has as its primary aim to construct and calibrate an instrument capable of detecting small changes in electrical conductivity. The calibration would be electrical conductivity versus some electrical parameter (current, voltage, etc.). To achieve this aim, two sets of experiments were run using two different coils and bridge arrangements. Both experiments used cores of three different materials: brass, copper, and aluminum.

The first experiment consisted of a standard general radio bridge , (250 A), arranged as a Maxwell bridge, to measure Q and L of the coil, both with and without the conducting cores. Due to the low Q of the coil and the skin depth limit on frequency, the bridge was unable to detect any changes in output due to core conductivity. The operation was also limited because of the bridge sensitivity being frequency dependent. This reduced the accuracy of the bridge at low frequencies to a level insufficient for detection of the theoretically small changes in output voltage. Therefore, another bridge arrangement was tested with a new set of coils.

This new bridge, referred to as a nonlinear twin T type of bridge, is discussed by Lion (18) and Földvári (19). This

bridge has the advantages of:

a) Higher sensitivity than standard Maxwell bridge.

b) Maximum bridge sensitivity is independent of frequency

c) Common ground for input and output

d) Output is D.C.--no rectification needed

e) Simple construction

Two matched coils of a higher Q were constructed and matched to the bridge circuit. Cores of aluminum, brass, and copper were used to obtain the variations in σ. Changes in bridge output were detectable with this arrangement, but instrument sensitivity and accuracy were seemingly not adequate for calibration. Qualitative agreement could be obtained, but quantitative agreement was poor. A more thorough analysis of the theory and operation of this experimental phase will be presented and will explain some of the discrepancies.

Since this later phase provided the only substantial data, the first experiment will be passed over with the previous comments.

4.1 Nonlinear Twin T Bridge

The twin T bridge is essentially a bridge of two unbalalanced arms, the measure of the unbalance being correlated

with the variable of interest. For the inductive bridge, a complete review of the theory is given in Reference 19. Referring to the following sketch,

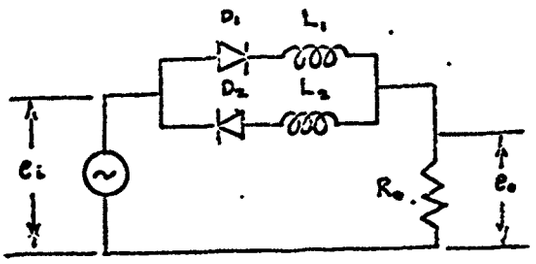

the bridge consists of two arms, each containing a diode and one of two identical coils. By applying an alternating voltage, the bridge arms are alternately conducting and open due to the diode action. In the conducting arm, the current in the coil builds at a certain rate depending on the time constant of this arm, while the current in the other arm decays, since it is an open circuit. On the opposite half-cycle, the reverse happens. If the D.C. value of e_o is taken for a balanced bridge, current in both coils builds up at the same rate, their output voltage being of opposite polarity. The sum of the D.C. voltages is zero. For the unbalanced case, a non zero reading of E_o is obtained. Assuming an applied square wave voltage, the circuit may be

represented for each half cycle as,

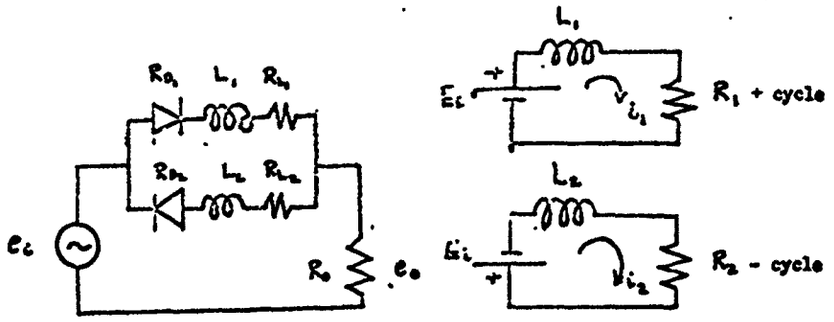

For each of these linear circuits, the current pattern for the half cycle can be represented as,

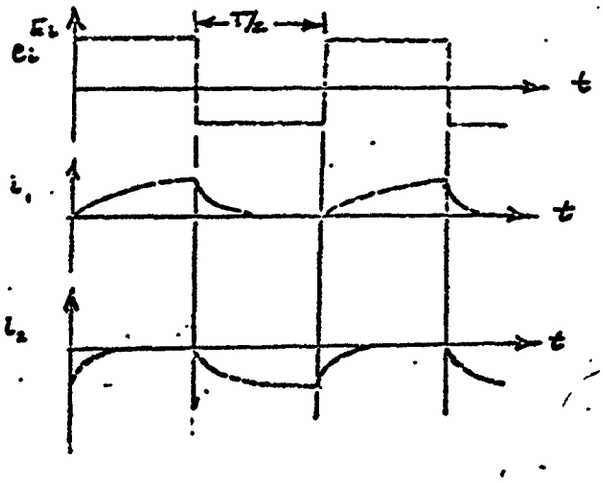

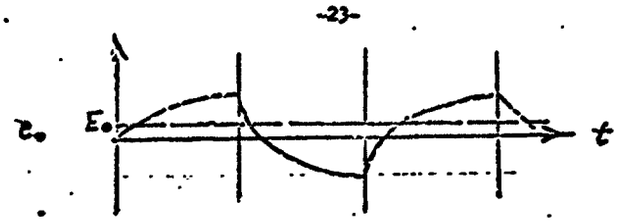

A circuit analysis of each half cycle, assuming that the current during the open portion decays to zero immediately, was carried out by solving for currents i_1 and i_2 as a function of the half period, $T/2$. The time average of the sum of the currents through R_o represents the D.C. output of the bridge. This expression is,

$$\frac{E_o}{E_i} = \frac{R_o}{2}\left[\frac{R_2 - R_1}{R_1 R_2}\right] + \frac{R_o}{2}\left[\frac{2fL_1}{R_1^2}\left(e^{-\frac{R_1}{2L_1 f}} - 1\right) - \frac{2fL_2}{R_2^2}\left(e^{-\frac{R_2}{2L_2 f}} - 1\right)\right]$$

where R_1 represents the total resistance of the (+) half cycle circuit.

$$R_1 = R_{D_1} + R_{L_1} + R_s + R_o$$

R_{D_1} = Diode forward resistance

R_s = Source resistance

R_o = Output resistor

R_{L_1} = Coil resistance

The coil resistance is equal to the total resistance of the coil windings plus the resistance induced in the core. Initially, both coils have an air core. Then one is replaced with a core of a finite conductivity. R_2 will differ in each arm of the circuit between these two situations. The resulting amount of unbalance, as recorded by the D.C. output, can be calibrated with the core material conductivity. With the present theory, R_L is given by,

$$R_L = \Omega \left[1 + \frac{\omega^2}{\Omega} \left(\frac{\mu_0 \sigma r_c^2 L_c}{8} \right) \right]$$

In terms of Q and ϵ_i, R_L is,

$$R_L = \Omega \left[1 + \frac{Q \epsilon_i^2}{4} \right]$$

However, due to the switching action of the diodes in the circuit, one of the basic assumptions of a sinusoidal steady state is no longer strictly true. Thus R_L must be modified for this condition by the ratio factor (Appendix B).

Another modifying factor, C, is introduced to account for other non ideal parameters of the circuit. With both these modifications R_L is,

$$R_L = \Omega \left[1 + \frac{Q \epsilon_i^2}{4} \cdot \text{RATIO} \cdot C \right]$$

where ratio $\equiv \frac{\text{Magnetic energy to coil}}{\text{Maximum energy to coil}} \equiv 1 - 2e^{-\frac{R}{Lf}} + e^{-\frac{2R}{Lf}}$

$C \equiv$ Non ideal circuit parameter correction

Appendix (B) explains more fully both these parameters.

4.2 Bridge Sensitivity

The bridge voltage sensitivity can be defined as the change in output voltage due to a change in the resistance of one arm. Since the output voltage is across R_o, it is necessary to separate R_o from the total R. R will be defined as,

$$R = R_{D_1} + R_L + R_s + R_o = r + R_o$$

Dividing both sides by a $(2Lf)$ factor this is now defined as a type of Q for the bridge.

$$\frac{R}{2Lf} = \frac{r}{2Lf} + \frac{R_o}{2Lf}$$

Keeping R_2 constant and assuming $L_1 = L_2$, R_1 is allowed to vary by a change in r_1. Taking the partial derivative of E_o with respect to r_1 the resulting expression is,

$$\frac{1}{Ei}\frac{\partial E_o}{\partial r_i} = + \frac{R_o}{(r_i+R_o)^2}\left\{\frac{1}{2} + \frac{2L_1f}{(r_i+R_o)} + L_1 f e^{-\frac{r_i+R_o}{2L_1f}}\left[\quad\right]\right\}$$

where $\left[\quad\right] \equiv \frac{r_i}{(2L_1f)^2} + \frac{1}{r_i+R_o}$

By defining $k = \frac{r_1 + R_o}{2L_1 f}$

$$k_1 = \frac{r_1}{2L_1 f}$$

$$k_o = \frac{R_o}{2L_1 f}$$

Thus, $k = k_1 + k_o$ and $\frac{k_o}{k} = \frac{k_o/k_1}{1 + k_o/k_1}$.

Defining the voltage sensitivity S_v as

$$S_v = \frac{\partial E_o}{\partial r_1}$$

the above equation can be written as,

$$S_v\left(\frac{2L_1 f}{E_i}\right) = \left(\frac{k_o}{k}\right)\left\{\frac{1}{2k} + \frac{1}{k^2} + e^{-\frac{1}{2}}\left[\frac{1}{2} - \frac{1}{k^2} + \frac{1}{2k}\left(\frac{k_o}{k}\right)\right]\right\}$$

A numerical evaluation appears in Figure (6). Some interesting conclusions can be drawn from this equation by looking at the limits of S_v as k and k_o go from zero to infinity.

a) for constant k_o as,

$k \to k_o$ $\quad S_v \to$ limiting value

$k \to \infty$ $\quad S_v \to 0$

b) for constant k as,

$k_o \to 0$ $\quad S_v \to 0$

$k_o \to \infty$ $\quad S_v \to 0$ since $\frac{k_o}{k} \to 1.0$

Graphically this can be represented by ,

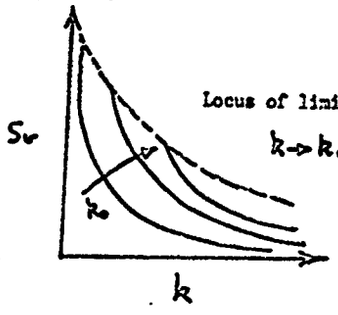

Locus of limiting S_v as $k \to k_o$

Figure 6

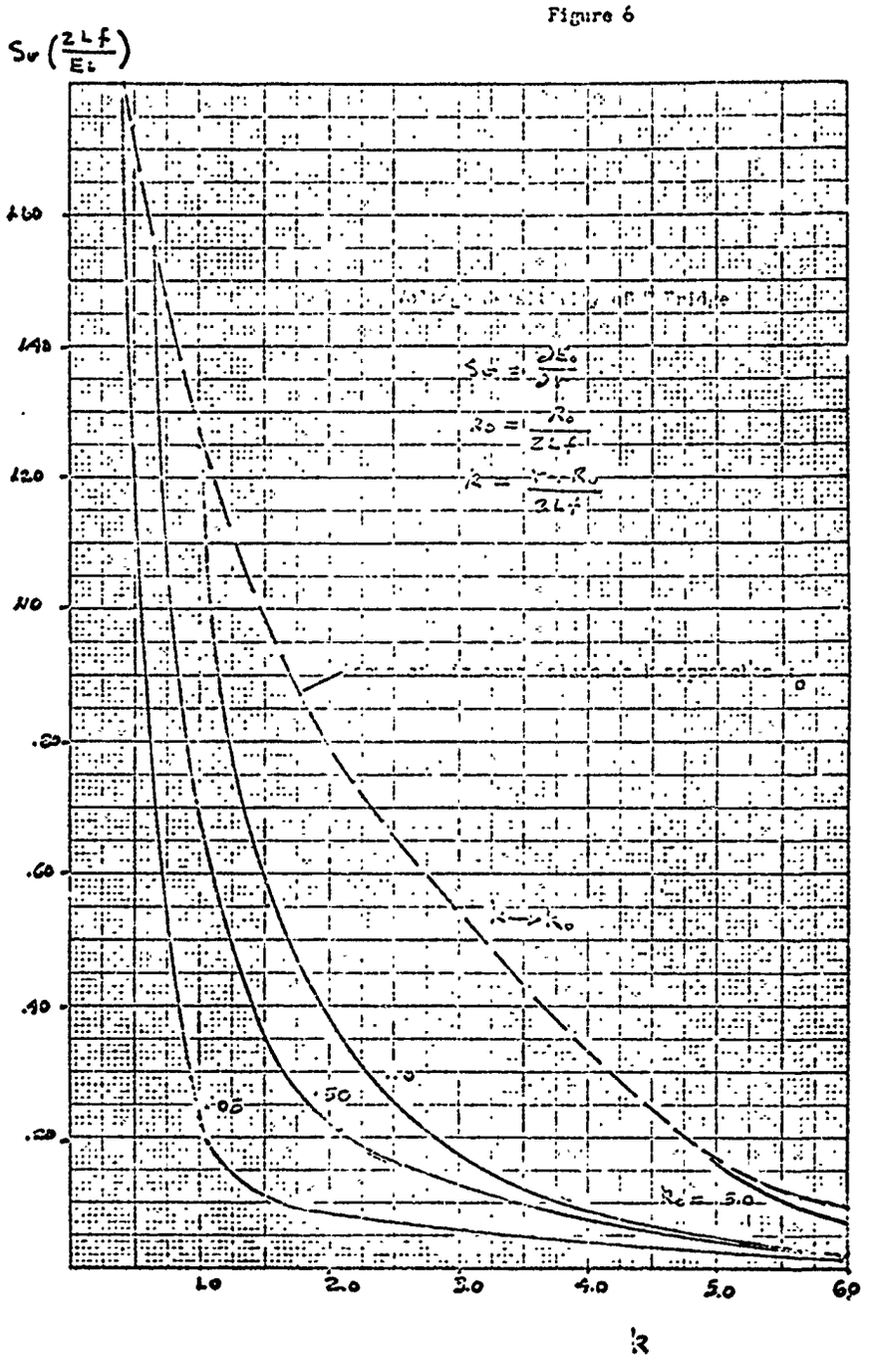
$S_v\left(\frac{2Lf}{E_i}\right)$
1.60
1.40
1.20
1.00
.80
.60
.40
.20
1.0
2.0
3.0
4.0
5.0
6.0
R
$S_v = \frac{2L}{\lambda}$
$R_0 = \frac{R_0}{2Lf}$
$R = \frac{R_0}{2Lf}$
$R_c = 5.0$
.50
.05

Thus, a low value of k is desirable for maximum bridge sensitivity. Yet for a given value of k_1, sensitivity can be increased by increasing k_o up to a point.

Since k increases with k_o, increasing k_o tends to decrease S_v. Thus an optimum R at which S_v is a maximum will occur.

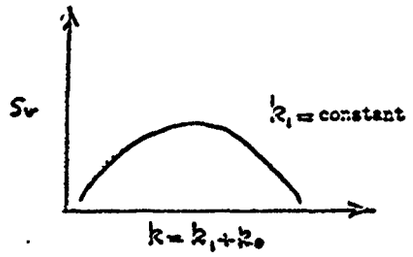

4.3 Experimental Arrangement

In order to achieve as high a sensitivity as possible, two higher Q coils were constructed. Both of these coils, as measured on a general radio 1650-A bridge, had an inductance of 6×10^{-3} Henries with a Q of one being 10 and the other 12 at 1000 CPS. Due to winding difficulties the L was reduced from the theoretical value. Figure (7) shows the coil dimensions and parameters. One coil was constructed to accomodate the removable 1/4 inch metal core, while the other remained an air core.

The bridge was constructed using number A-D junction diodes of the following characteristics:

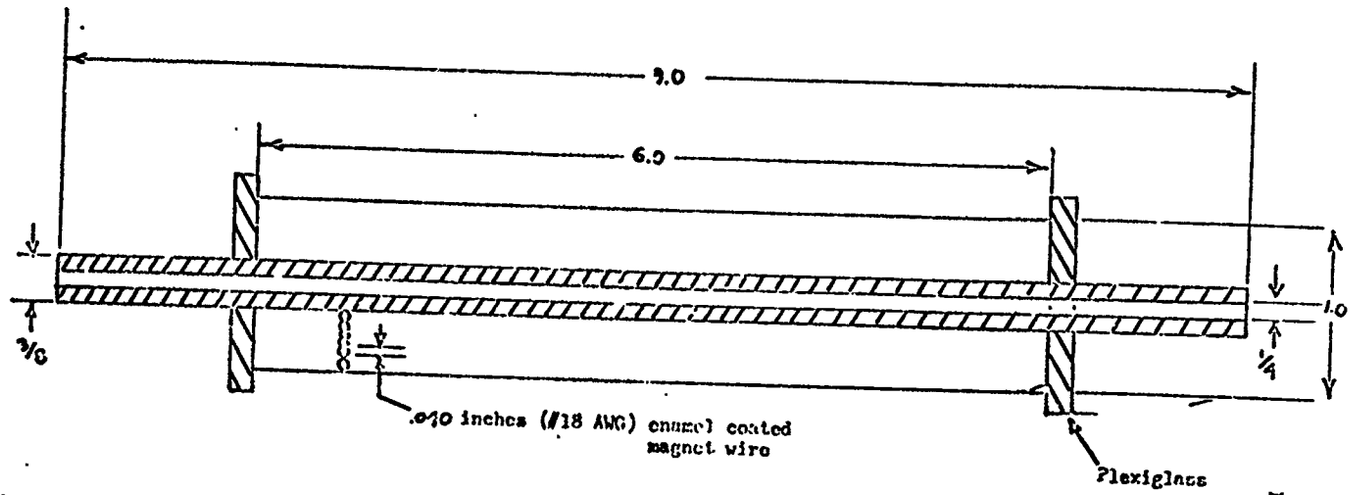

	COIL 1	COIL 2
L	6×10^{-3}	6×10^{-3}
Ω	4.8	4.0
Q	10.0	12.0

at 1000 cps
Turns = 2000
Layers = 13

Induction Coil
Geometry and Parameters

Figure 7

PIV = 200 Volts

$I_{D\ C\ max} = 1$ Amp

$I_{FWD\ at\ 1\ Volt} = 1$ Amp

Thus, the diodes had a fairly sharp cutoff point and a high value of limiting current. Their forward resistance was 1 Ohm.

The output resistance was varied by using a general radio decade resistance 602-M box, with decades from 10^0 to 10^3. A balance resistor R_B, consisting of a slide wire resistor with a maximum resistance of .90 Ohm was used to balance the circuit to the same original DC voltage reading. Both the slide wire and decade box were outside the bridge itself, the bridge box consisting of the two coils and the diodes. Figure (8) shows the basic bridge circuit.

Due to difficulties in maintaining a stable input square wave signal, a clipper circuit was built to insure a constant voltage to the amplifier. This is shown in Figure (9).

The experimental circuit is shown in Figure (10) and contained the following equipment:

a) General radio power supply 1203-B with GR R-L oscillator 1210-C 0-30 Volt peak square wave input signal.

b) Clipper-maximum voltage of 6.75 volts supplied by mercury batteries with a variable resistor to control the voltage to the amplifier

Figure 8

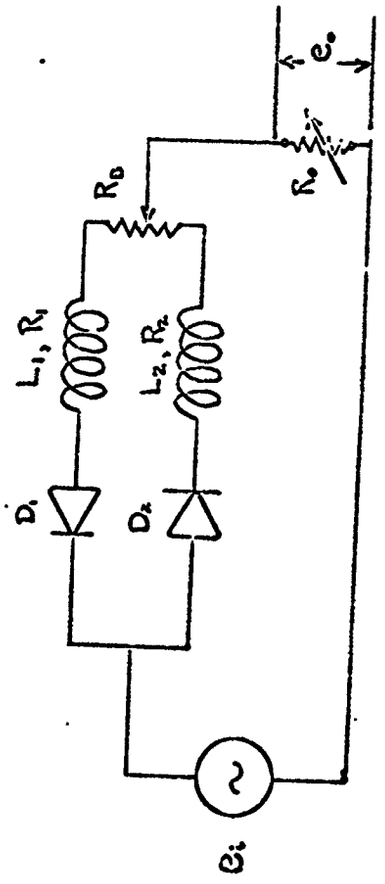

T Bridge Circuit

Figure 9

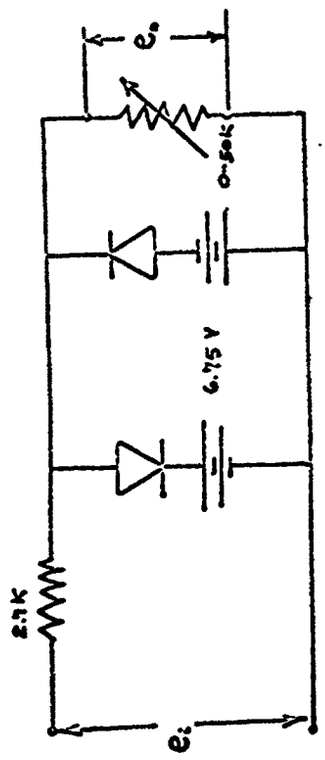

Clipper Circuit

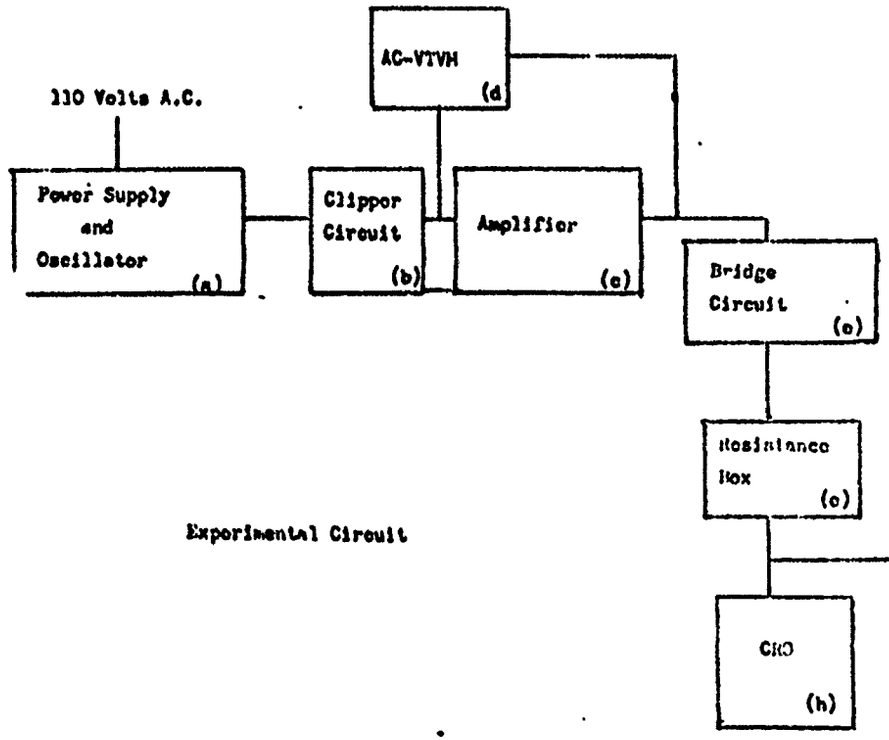

Experimental Circuit

Figure 10

c) Dyankit audio amplifier--gain constant at about 10. 4 Ω output terminal used to provide low input impedance for the bridge circuit

d) Hewlett-Packard AC VTVM-400D to measure e_i into bridge

e) Bridge with decade box and balance resistor. Low decades used to maintain a low R_o

f) Hewlett-Packard AC VTVM-400D to measure e_o of bridge

g) Hewlett-Packard DC VTVM-412A to record the D.C. output of the bridge E_o, due to the unbalance. Low scale reading to 1×10^{-3} volts.

h) Hewlett-Packard CRO-150B to monitor output wave form pattern as well as check input wave form.

The cores were made of copper, brass, and aluminum, all of at ut 12 in. long and 1/4 in. diameter. These represented an approximate range of conductivity values of (Reference 23):

Copper = 6.3×10^7 MHO/meter

Aluminum = 3.6×10^7 MHO/meter

Brass = 1.43×10^7 MHO/meter

4.4 Experimental Procedure

The basic procedure was: at a value of frequency, to set e_i and record E_o with both cores air; then, to place a metal core in the variable coil and record E_o again. This

core was then removed, and the frequency set to a new value. e_i was maintained at the same initial value and the procedure continued with the same metal core. Only one core at a time was tested, and then the same procedure was repeated for the next core with the same value of e_i as the original core. R_o was maintained constant throughout the series of tests of all three cores.

Tests were carried out for both the square wave (with clipper) and sine wave (without clipper) inputs. Since the sine wave input proved superior in results, only this case will be presented and discussed. The bridge circuit was optimized for maximum voltage sensitivity with a sine wave input. This caused an output resistor R_o of 7.5 Ohms to be used in the circuit. Inadequate instrumentation prohibited any experimental verification of this as the optimum load resistor.

4.5 Experimental Data

Data was obtained for the T bridge using the three metal cores. This data was in the form of voltage output of the bridge for air and then metal core in the coil. Unfortunately, the data was not extensive or good. Difficulty was experienced with the instrumentation in obtaining definite and repetitive readings; the readings were not definite because the output tended

to be unstable, oscillating around some mean point. It usually exhibited a swing of $\pm 1/2 \times 10^{-3}$ volts. The readings were not repetitive since in many instances the output would drift or not give the same readings when repeated at the same frequency. Possible solutions of these difficulties will be suggested further on.

Data for both sine and square wave inputs were taken, (Appendix C), but as a result of the uncertain readings, only one set of data, that for the sine wave, is discussed.

Appendix (C) lists the data obtained. All readings are the mean readings of the voltage output. Figures (11) and (12) show a plot of this data.

Another limitation on the data obtained was the limited range of the output metering. At low scale readings, instability caused poor readings, while at high scale readings, lack of adequate D.C. vacuum tube volt meter sensitivity was the main limitation.

In the following section, a highly limited comparison is made between this set of data and the predictions of the theory.

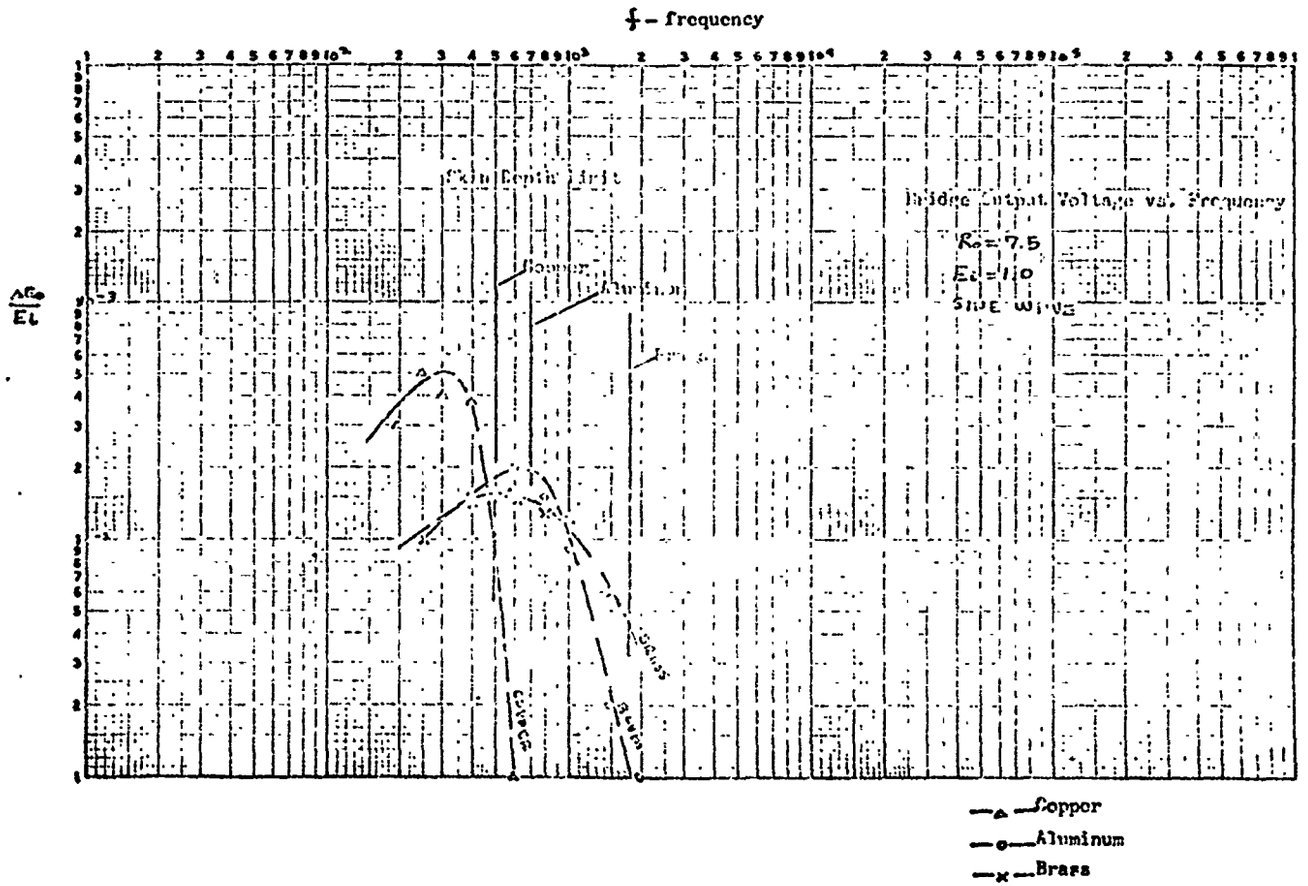
f – Frequency
Skin Depth Limit
Bridge Output Voltage vs. Frequency
R_o = 7.5
E_i = 10
Copper
Aluminum
Brass
—△— Copper
—○— Aluminum
—×— Brass

Figure 11

Figure 12

Bridge Output Voltage versus Frequency

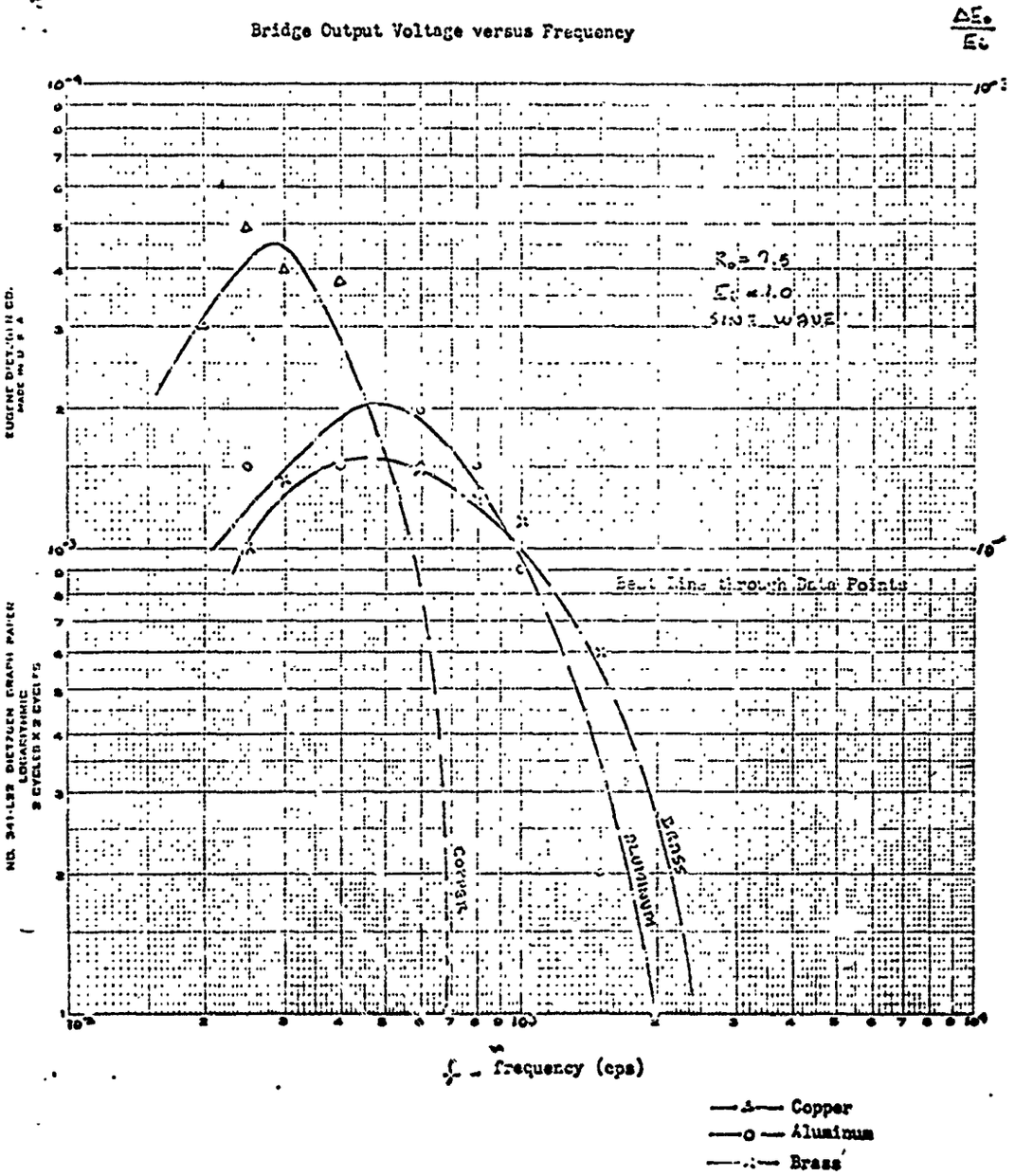

5.0 Theoretical and Experimental Comparison

In order to more fully explore the range of the theoretical predictions, a digital computer program was employed. This program calculated bridge output as a function of frequency for various combinations of coil and core parameters. The equation for bridge output,

$$\frac{E_o}{E_i} = \frac{R_o}{2}\left[\frac{R_2 - R_1}{R_1 R_2} + \frac{2L_1\zeta}{R_1^2}\left(e^{-\frac{R_1}{2L_1\zeta}} - 1\right) - \frac{2L_2\zeta}{R_2^2}\left(e^{-\frac{R_2}{2L_2\zeta}} - 1\right)\right]$$

where $R_{1,2} = R_S + R_D + R_o + R_L$

and $R_L = \Omega\left[1 + \frac{\omega^2}{\Omega^2}\cdot\frac{\mu_o\sigma\pi^2 L}{3}\cdot RATIO\cdot C\right]$

was programmed in Fortran for the IBM 7090. An evaluation was then carried out to attempt to match experimental and theoretical values. For the data in question, the theoretical calculations assumed the following values:

R_o = 7.5 ohms

$R_{D1} = R_{D2}$ = 0 ohms

$\Omega_1 = \Omega_2$ = 4.0 ohms

$L_1 = L_2$ = 6.0 millihenries

σ_1 = 0 Mho/meter

σ_2 = 6.3×10^7 Copper, 3.6×10^7 Aluminum
1.4×10^7 Brass--Mho/meter

Figure (13) shows a comparative plot for a value of C = 1.0.

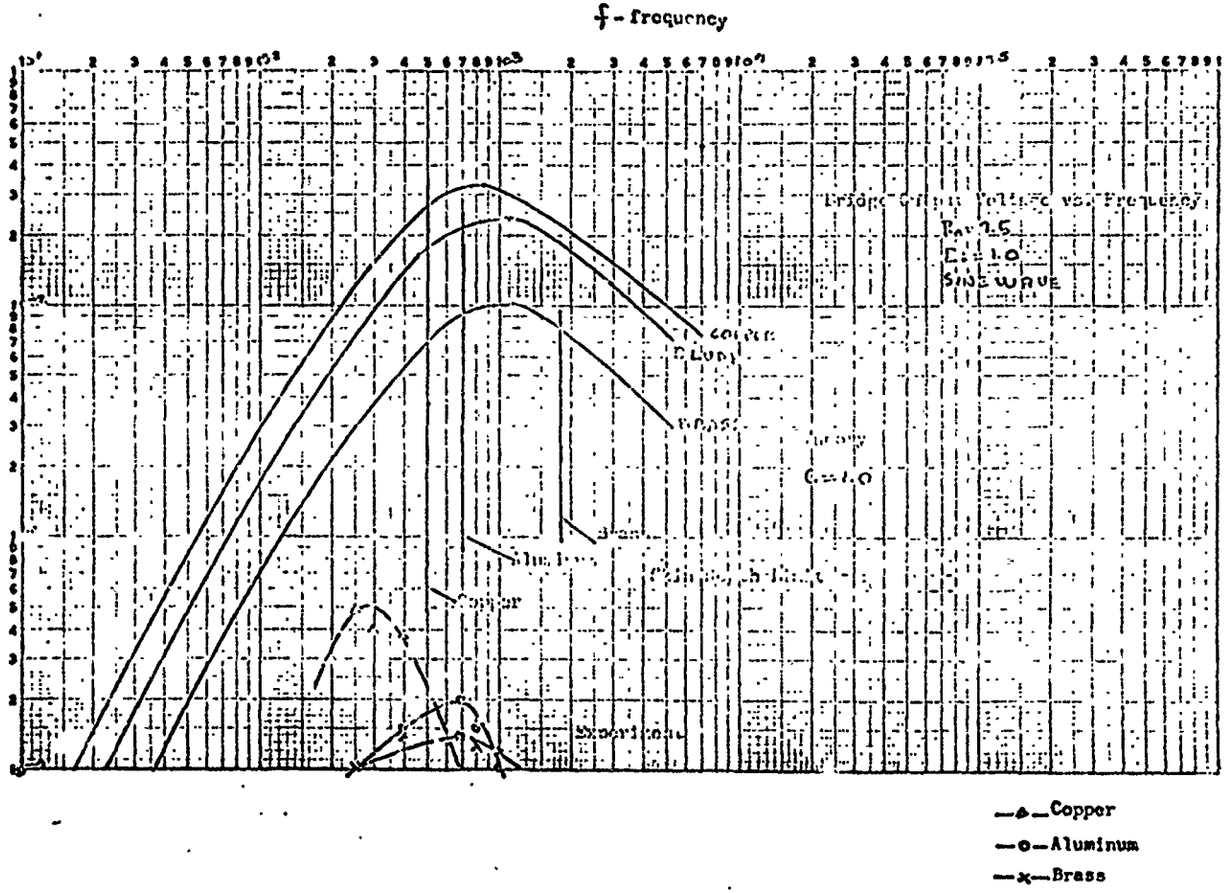

Figure 13

Agreement is obviously quantitatively poor but qualitatively good. Before discussing results for different values of C, a better understanding of some of the limitations of the theory is needed.

Upon comparing data and theory it is noted that both curves follow closely in qualitative nature. Both display maximums in the same frequency range and their order in magnitude is as predicted. But unfortunately, the differences overshadow the similarities. It must be emphasized that the theoretical predictions are only valid up to the frequency where $r_c = \delta$, the skin depth limit. For the three cores used, this frequency is:

Copper $\approx$ 500 cps

Aluminum $\approx$ 700 cps

Brass $\approx$ 1800 cps

as noted in Figures (13) and (14).

Note first the rapid decrease in the data at higher frequencies as compared to the theory. This is due to the skin depth limitation that is unaccountable in the theory. Since the theoretical relationship between $R_L = f(\omega,\sigma)$ is valid only up to the frequency at which $\delta = r_c$, it is restricted to frequencies below this critical frequency. After this frequency is exceeded, L changed and an unbalance now existed, due not only to R but also to L. But, past this frequency limit the change in R becomes less since the fields are now excluded form the core. Thus, there is less induced resistance than predicted by the present theory. The fact that the induced

resistance becomes a maximum near the initial frequency is an important limitation that is not reflected in the present theory. Since this critical frequency varies with core conductivity, the point at which L starts to diminish and the bridge ceases to record just changes due to R, will vary with core material. As L gets less, (E_o/E_i) will tend to decrease even faster, due to a more rapidly decreasing (L/R_1) in the vicinity of the critical frequency. Thus, the output can be expected to cross the axis at some point dependent on the critical frequency. Since the critical frequency decreases with a higher conducting material, this cross-over point can be expected to shift to the right with lower values of σ. In the limit, thus, as $\sigma \to 0$ this point will be at infinity. Thus $(\Delta E_o / E_i)$ experimental can be schematically represented as,

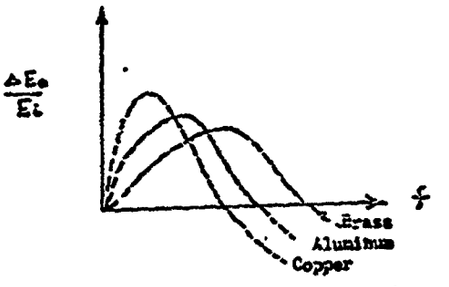

This rapid decrease as well as the exclusion of the $\underline{E}$ fields from the core at higher frequencies are two important effects that effect not only the shift in peak of the data and theory, but also the magnitude of the output. In closing the discussion of the skin depth limitation, it should be noted as set forth in Appendix (B) that a true sinusoidal steady state does not exist due to the diode action. Since skin depth is defined on a sinusoidal steady state basis, this too would be somewhat effected by the non-sinusoidal behavior.

The quantitative difference between theory and experiment is the next point in question, one that is not easily resolved. Figure (13) shows approximately two orders of magnitude difference between the theory and data. Figure (14) shows theory and experiment for C = .01. The shift in peaks is due to the skin depth limitation as postulated previously. This means that either the theory predicts values of induced resistance 100 times greater than is actually the case, or the theory is wrong. There are several possible places that this discrepancy could arise:

1. Inconsistency in square wave derivation of bridge equations and sinusoidal derivation of R_2
2. Incorrectness of R_L due to skin depth limitation
3. Losses within the actual circuit not accounted for in the theory except by use of the factor C

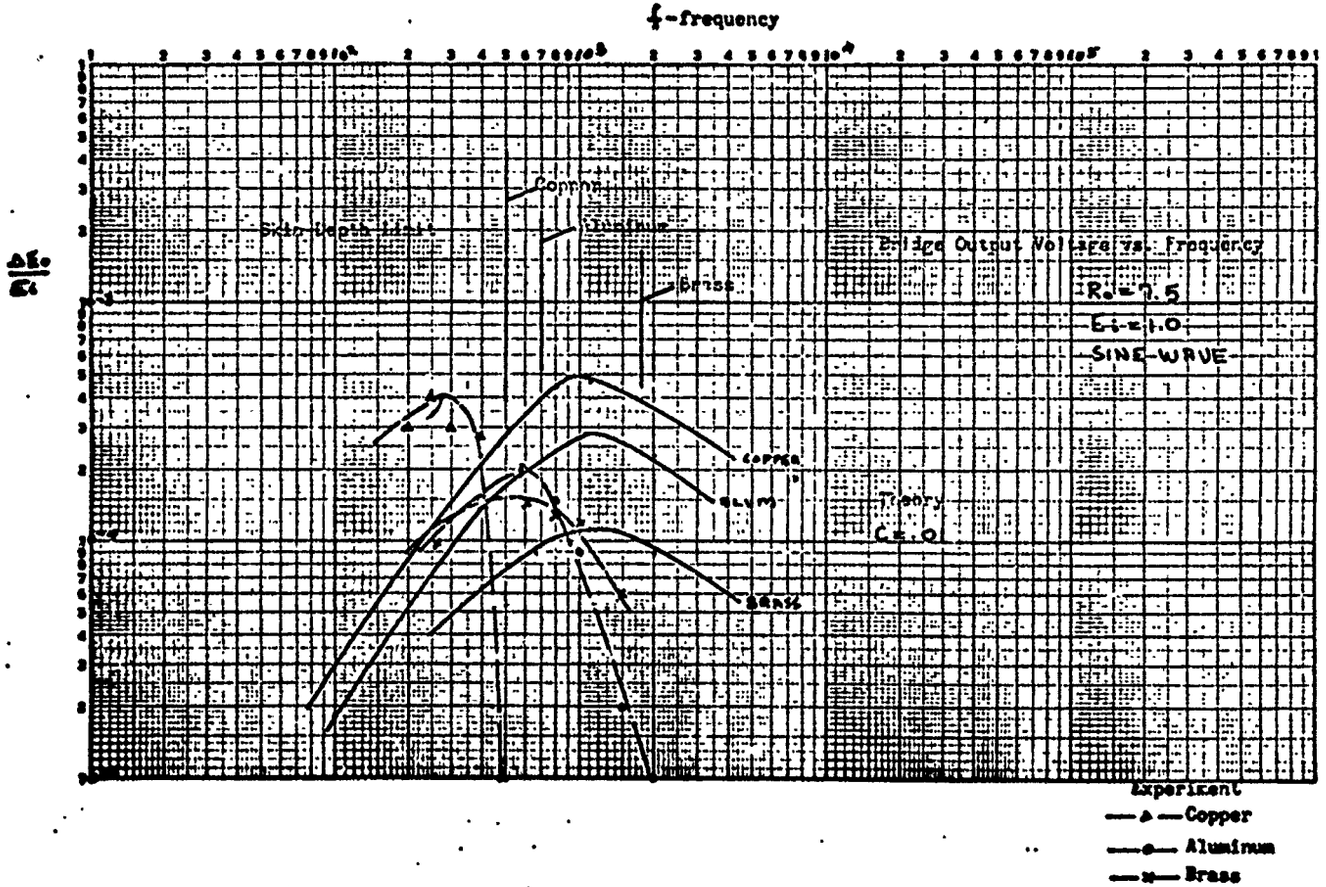

Figure 14

The first possibility should not cause any significant differences, since the bridge equations should be of the same general form.

The second possibility is hard to evaluate without a full derivation of an analysis including the skin depth. If the bridge equation is of the same form in the light of 1., a small change in R_2 can strongly effect the magnitude of $\Delta E_o / E_i$ due to the nature of the equation. An indication of the change is given by the curve of bridge voltage sensitivity at low values of R.

As hypothesized in Appendix (5), the factor C is assumed to account for losses of power in the bridge that could reduce the power to the coil, and thus the strength of the induced field within the coil core. These losses include: contact resistances, mutual inductance between coils, unbalances in $L_1 \neq L_2$ and $\Omega_1 \neq \Omega_2$. However, all of them would appear to be small effects, and not sizeable enough to cause a reduction of a factor of 100 in bridge performance. Theoretical results have indicated that an unbalance in L of 10 % causes a reduction in output of about 6%, while an unbalance in Ω of 25% causes a reduction of about 5%. The mutual inductance between the coils reduces the power to the coils, therefore also reducing the sensitivity and output. The magnitude of this change is not known, but it would seem to be small for

the coils and field strengths involved here. Thus, the factors which C is related to, would appear to be of a secondary nature.

Until better data is obtained, nothing positive can be formulated as to the correctness or incorrectness of the theory. Since better data is primary to any reliable calibration, a need for a revision of the theory would be dependent on this data.

Turn for a moment to the reasoning that the theory is correct but that the data wrong. This has as its only support the possibility of faulty bridge or coil construction. This will be proved or disproved only upon construction of a new bridge and obtaining of new and better data.

6.0 Conclusions

Conclusions can be very briefly summarized as follows: using a nonlinear twin T type of bridge in conjunction with an induction coil technique, a method of determining the relative electrical conductivity between highly conducting materials has been developed. At present, the theoretical basis of the method agrees only in a qualitative way with the small amount of data obtained in this preliminary study. No satisfactory explanation as to the quantitative differences has yet been formulated. However, it is important to note that in the eventual development of an instrument, theoretical and experimental agreement is but a point of satisfaction, since the primary concern is an accurate and repeatable calibration from which the unknown conductivity of a material can then be determined. The initial goal of this study was to determine the equivalent electrical conductivity of a two phase liquid metal flow. This directly, has not been achieved. However, the present technique represents an initial step in that direction.

7.0 Bibliography

1. Elliot, D.G., "Liquid MHD Power Conversion", JPL Space Programs Summary, #37-71, 1963.

2. Jackson, N.D. and Brown, G.A., "Liquid Metal MHD Power Generator Utilizing the Condensing Ejector", Patent Disclosure, M.I.T., October 15, 1962.

3. Lee, K. S., "Analysis of an MHD Power Generation System for Liquid Metals", S.M. Thesis, Department of Mechanical Engineering, M.I.T., January, 1964.

4. Weber, H.E., and Marston, C.H., "Liquid Metal Vortex MHD Generator", ASME 63-WA-209, Winter Annual Meeting, Philadelphia, Pa., Nov. 17-22, 1963.

5. Maxwell, J.C., "A Treatise on Electricity and Magnetism", Vol. I, Chap. IX, pg. 435, Dover Edition.

6. Merodith, R. E., "Resistance to Potential Flow through a Cubical Array of Spheres", Journal of Applied Physics, Vol. 31, No. 7, July 1960, pg. 1226.

7. Fricke, H., "A Mathematical Treatment of the Electrical Conductivity and Capacity of Disperse Systems", Physical Review, Vol. 29, 1924, pg. 575.

8. Nickerov, A.E., "The Electrical Conductivity of Alloys Forming a Mechanical Mixture", Soviet Physics-Technical, No. 2, 1957, pg. 1892.

9. Korneenko, I.A., "Mean Values of the Parameters in Inhomogeneous Media", Soviet Physics-Technical, No. 5, 1961, pg. 40.

10. Pliat, S.N., "Extension of Opalevskii's Theory of Generalized Conductivity to Thermal Conductivity", Soviet Physics-Technical, No. 2, 1957, pg. 2588.

11. Fano, R.M. et.al., Electromagnetic Fields, Energy, and Forces , John Wiley, New York, 1963.

12. Fitzgerald, A.E., Basic Electrical Engineering, McGraw-Hill, New York, 1957.

14. Lin, S.C., et.al., "Electrical Conductivity of Highly Ionized Argon Perduced by Shock Waves", Journal of Applied Physics, Vol. 26, No. 1, Jan., 1955, pg. 95.

15. Korvitz, H.E., "Technique for Measuring the Conductivity of Wakes of Projectiles at Hypersonic Speeds", Review of Scientific Instruments, Vol. 35, No. 2, Feb., 1964, pg. 201.

16. Donskoi, K.V., "Measurement of Electrical Conductivity in Gas Streams", Soviet Physics-Technical, Vol. 7, No. 9, 1963.

18. Lion, K., "Nonlinear Twin-T Network for Capacitive Transducers", Review of Scientific Instruments, Vol. 35, No. 3, March, 1964, pg. 353.

19. Földvari, T., "Measuring Method for Inductive and Molecular Transducers", MS. Thesis, M.I.T., 1963.

20. Wallis, G., "Some Hydrodynamic Aspects of Two Phase Flow and Boiling", International Heat Transfer Conference, 1961, Part II, Pg. 319.

21. Zuber, N., "Steady State and Transient Void Fraction of Bubbling Systems and Their Operating Limits", General Electric Engineering Lab Report, 62G-L100, July 1, 1962

22. Haus, H., Gas Studies in Electrochemistry, John Wiley & Sons, New York, 1960.

23. Handbook of Chemistry and Physics, 44 Edition, 1963, Chemical Rubber Publishing Co., Cleveland, Ohio.

Appendix A Electro-magnetic Field Relationships on a Cylindrical Coil

Referring to the geometry of the following figure,

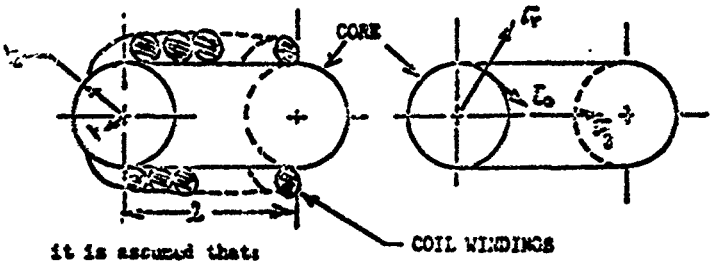

it is assumed that:

1. The skin depth is not exceeded, $\delta \leq r_o$
2. Negligible displacement current, $\sigma >> \omega \epsilon_o$
3. [illegible]
4. The coil windings can be approximated by a zero order, time-varying current sheet of magnitude $\left[\frac{NI_o}{\ell}\right]$ at $r = r_o$
5. The coil windings are of infinite conductivity.
6. The core is of non-magnetic material: $\mu = \mu_o$
7. Assume a sinusoidal steady state exists. Thus all time-varying quantities can be represented, in complex notation, as proportional to $e^{j\omega t}$
8. Neglect all field external to $r = r_o$.
9. The solution can be carried out in a form of successive approximations, i.e., by assuming

the total field is the sum of an infinite series consisting of terms of differing degrees of time-variation (See Reference 11, Fano, Chap. 6). Thus,

$$\bar{\underline{\underline{E}}} = \bar{\underline{\underline{E}}}_0 + \bar{\underline{\underline{E}}}_1 + \bar{\underline{\underline{E}}}_2 + \ldots \text{ etc.}$$

where subscripted terms will be referred to as the zero order, first order, second order, etc. of the field.

The following notation will be adopted:

a) Single sub bar--complex quantity $\underline{K}$

b) Single super bar--vector quantity $\bar{K}$

c) Super and sub bar--complex vector $\bar{\underline{K}}$

Thus, $\bar{K}_0 = K_0 \cos\omega t$, introducing complex notation becomes,

$$\bar{K} = \tfrac{1}{2}\left[\underline{K}_0 e^{j\omega t} + \underline{K}_0^{*} e^{-j\omega t}\right]$$

where $\underline{K}_0^{*}$ is the complex conjugate of $\underline{K}_0$.

All units will be in the rational MKS system. In conceptual form, the zero order current will cause a zero order magnetic field. This in turn induces a first order electric field composed of a solenoidal field due to the zero order magnetic field and a conservative reaction field due to an induced surface charge. The solenoidal field in turn induces a first order magnetic field, thus giving rise to a second order

electric field in the core. Once the proper field relationships are established, Poynting's theorem can be used to determine the power flow into a control surface around the core since the fields outside the core are neglected. From this, the time-average power relationships for the coil due to the applied and induced fields, can be derived.

Throughout the analysis the notation of Reference 11 will be adhered to. All quantities will be of a complex time-varying nature.

Zero Order Fields

The zero order Maxwell's equations are,

$$\nabla \times \bar{E}_0 = 0$$

$$\nabla \times \bar{H}_0 = 0$$

$$\nabla \cdot \bar{J}_0 = 0$$

$$\nabla \cdot \bar{E}_0 = 0$$

$$\nabla \cdot \mu_0 \bar{H}_0 = 0$$

By assumption $\bar{E}_0$, $\bar{J}_0$ are both zero within the core and with an applied current sheet at $r = r_c$ of,

$$\bar{K}_0 = \hat{i}_\theta \left[\frac{N I_0}{\ell} \right]$$

From the second relationship and boundary conditions, the zero order magnetic field is,

$$\bar{H}_0 = \hat{i}_\theta \left[\frac{N I_0}{\ell} \right]$$

First Order Fields

$$\nabla \times \bar{E}_1 = -j\omega\mu_0 \bar{H}_0$$

$$\nabla \cdot \epsilon_0 \bar{E}_1 = 0$$

$$\nabla \cdot \mu_0 \bar{H}_1 = 0$$

$$\nabla \times \bar{H}_1 = \bar{J}_1 + j\omega\epsilon_0 \bar{E}_0$$

$$\nabla \cdot \bar{J}_1 = 0$$

In solving for the electric field, it is noted that at the surface $r = r_c$, $\bar{E}_1$ is composed of two parts, a conservative and solenoidal portion

$$\bar{E}_1 = \bar{E}_{1s} + \bar{E}_{1c}$$

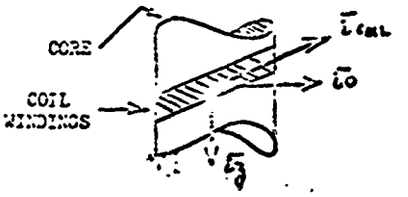

The conservative component arises from the induced surface charge in the coil which is required to meet the condition that no field exists within the coil windings ($\sigma_{coil} = \infty$). Solving for $\bar{E}_{1s}$ at $r = r_c$ from the equation,

$$\nabla \times \bar{E}_1 = -j\omega\mu_0 \bar{H}_0$$

results in,

$$\bar{E}_{1s} = \bar{i}_\theta\, j\omega\mu_0 \left[\frac{NI_0}{2}\right] \frac{r_c}{2}$$

From La Place's equation and the boundary condition of no field existing parallel to the coil direction ($\bar{i}_{coil}$ direction) $\bar{E}_{1c}$ can be solved for.

$$\bar{E}_{1\phi} = \bar{i}_\phi \, j\omega\mu_0 \frac{N\pi r_c^2}{\ell}\left[\frac{NI_0}{\ell}\right]\cos\left(\frac{\partial}{\partial z}\right)$$

With the voltage across the coil defined by ,

$$V_1 = \int_0^\ell \bar{E}_{1\phi}\, dz = \left[(\phi_z)_\ell - (\phi_z)_0\right]$$

Substituting for $\bar{E}_{1\phi}$, V_1 becomes,

$$V_1 = j\omega\mu_0 \pi r_c^2 \frac{N^2 I_0}{\ell}$$

For a cylindrical coil of infinite length, the inductance L, can be defined as

$$L = \frac{\pi r_c^2 \mu_0 N^2}{\ell}$$

Thus V_1 becomes,

$$V_1 = j\omega L I_0 = L\frac{dI_0}{dt}$$

which is the Faraday Induction Law relationship. Continuing the solution for the first order fields, the first order magnetic field is solved from,

$$\nabla \times \bar{H}_1 = \bar{J}_1$$

since $\bar{E}_0$ is zero. For a linear core material of conductivity (σ), $\bar{E}_1 = \bar{E}_{1\phi}$.

Thus, substituting for $\bar{E}_z$,

$$\bar{E}_2 = -\bar{\imath}_\phi \, j\omega\mu_0 \sigma \frac{r^2 N I_0}{4\pi}$$

Thus, the effect of a finite core conductivity is seen to enter into the analysis. Note that this is not valid for cases in which σ is such that $r^2 \gg \frac{4}{\omega\mu_0\sigma}$. A solution for this case can be carried out similarly to that found in Haus (Reference 22, pg. 205).

Second Order Fields

In order to complete the derivation of the fields required for application of the Poynting theorem, the second order electric field is needed. This is given by,

$$\nabla \times \bar{E}_2 = -j\omega\mu_0 \bar{H}_0$$

Solving for E_2 within the core,

$$\bar{E}_2 = -\bar{\imath}_\phi \, \omega^2\mu_0^2\sigma \frac{N I_0}{16\pi} r^3$$

Note that the induced E_2 field is proportional to σ and ω^4. Basically it is the real power due to ohmic losses caused by this field that causes the change in coil impedance due to the presence of a core of finite conductivity.

Power Relationships

Within the power series approximation, the total

Poynting vector is,

$$\bar{S} = \bar{S}_0 + \bar{S}_1 + \bar{S}_2 + \dots$$

where $\bar{S}$ the complex Poynting vector, can be found from

$$\nabla \cdot \bar{S}_0 = -\frac{1}{2}\left(\bar{E}_0 \cdot \bar{J}_0^*\right)$$

$$\nabla \cdot \bar{S}_1 = -\frac{1}{2}\left(\bar{E}_1 \cdot \bar{J}_0^* + \bar{E}_0 \cdot \bar{J}_1^*\right) - 2j\omega\left(\frac{1}{4}\mu_0 |\bar{H}_0|^2 - \frac{1}{4}\epsilon |\bar{E}_0|^2\right)$$

$$\nabla \cdot \bar{S}_2 = -\frac{1}{2}\left(\bar{J}_0^* \cdot \bar{E}_2 + \bar{E}_1 \cdot \bar{J}_1^* + \bar{E}_0 \cdot \bar{J}_2^*\right) - 2j\omega\left(\frac{1}{4}\mu_0 |\bar{H}_0 \cdot \bar{H}_1^* + \bar{H}_1 \cdot \bar{H}_0^*| - \frac{1}{4}\epsilon |\bar{E}_0 \cdot \bar{E}_1^* + \bar{E}_1 \cdot \bar{E}_0^*|\right)$$

Substituting the previously derived field expressions, and integrating the Poynting vector over the control surface of,

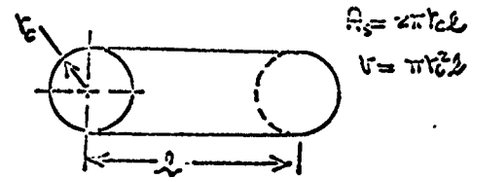

results in expressions for the time-average power dissipated in the control volume V

$$\langle P_0 \rangle = 0$$

$$\langle P_1 \rangle = 0$$

$$\langle Q_1 \rangle = j\omega\left[\frac{\mu_0 \pi r_c^2 N^2}{\ell}\right]\frac{I_0^2}{2} = \frac{1}{2}j\omega L I_0^2$$

$$\langle P_2 \rangle = \frac{\sigma\omega^2\mu_0^2}{8}\left[\frac{N I_0}{2}\right]^2 \pi r_c^4 \ell = \frac{\sigma\omega^2\mu_0}{8}\left[\frac{1}{2}L I_0^2\right] r_c^2$$

where $L \equiv \frac{\pi r_c^2 \mu_0 N^2}{\ell}$ and I_0 is the magnitude of the impressed current. The total time-average power supplied is,

$$\langle P_{in} \rangle = \frac{I_0 V_0}{2}$$

where V_0 is the terminal voltage impressed across the coil

If the coil has a finite resistance Ω, due to a non-infinite conductivity, the power loss due to this is,

$$\langle P_{coil} \rangle = \frac{I_0^2 \Omega}{2}$$

Equating the input power to that dissipated,

$$\langle P_{in} \rangle = \langle P_0 \rangle + \langle P_{coil} \rangle + \langle P_1 \rangle + \langle P_2 \rangle + \cdots$$

$$\frac{I_0 V_0}{2} = + \frac{I_0^2 \Omega}{2} + j\omega \left[\frac{1}{2} L I_0^2 \right] + \frac{\omega^2 \mu_0 \sigma r_c^2}{8} \left[\frac{1}{2} L I_0^2 \right]$$

Supplied Power	Resistive power Loss of coil	Reactive power loss of core	Induced resistive power loss of core

The magnitude of the power can be derived by combining real and imaginary parts. Thus.

$$\left(\frac{I_0 V_0}{2} \right)^2 = \frac{1}{4} L^2 I_0^2 \omega^2 \left[1 + \frac{\mu_0 \sigma r_c^2 \Omega}{2L} + \frac{\mu_0 \sigma \omega^2 r_c^4}{64} + \frac{\Omega^2}{\omega^2 L^2} \right]$$

noting that the coil impedance as seen across the coil terminals is defined as,

$$Z_0 = \frac{V_0}{I_0}$$

and defining the ratio of coil magnetic energy stored to the resistive power dissipated, as the ratio Q

$$Q = \frac{\omega L}{R}$$

this expression can be algebraically rearranged to,

$$\frac{Z_o}{R} = \left[Q^2 + 1 + Q \left(\frac{\omega \mu_o \sigma r_c^2}{8} \right) \left(Q \frac{\omega \mu_o \sigma r_c^2}{8} + 2 \right) \right]^{1/2}$$

From the definition of skin depth,

$$\delta = \left(\frac{2}{\omega \mu_o \sigma} \right)^{1/2}$$

this can be further reduced to,

$$\frac{Z_o}{R} = \left\{ Q^2 + 1 + \frac{Q}{4} \left(\frac{r_c}{\delta} \right)^2 \left[\frac{Q}{4} \left(\frac{r_c}{\delta} \right)^2 + 2 \right] \right\}^{1/2}$$

Defining the ratio of coil radius to skin d[illegible] as

$$\eta \equiv \left(\frac{r_c}{\delta} \right)$$

a final expression between equivalent coil impedance and the coil parameters is obtained.

$$\frac{Z_o}{R} = \left[Q^2 + 1 + \frac{Q \eta^2}{4} \left(\frac{Q \eta^2}{4} + 2 \right) \right]^{1/2}$$

Separating real and imaginary parts of the above expression yields the following equation for the total equivalent coil and core resistance

$$R_L = R \left[1 + \frac{Q \eta^2}{4} \right]$$

as given in the text.

Appendix B Effect of Non-Sinusoidal Steady State Behavior of the Bridge and Other Bridge Losses

A basic assumption in the derivation of the field equations for the coil is that a sinusoidal steady state exists in the coil-core combination. However, in the T bridge, the diode action causes the sinusoidal input to be switched before a full cycle is completed. Thus, a full sinusoidal steady state is not established. Some accounting of this reduction in power to the coils can be derived as follows.

For an input of zero frequency, the coil does receive the full steady state power, while for infinite frequency no power input goes into the coil. This power goes into the energy stored in the magnetic field plus the eddy current losses in the core. The energy in the magnetic field of the coil is given by $1/2\ L\ i^2$. If the bridge circuit is assumed to be an R-L circuit, the expression for current in the transient state is given by Fitzgerald (Reference 12, pg. 162)

$$i = I_0 \sin\left(\omega t - \tan^{-1}\frac{\omega L}{R}\right) - I_0 \sin\left(-\tan^{-1}\frac{\omega L}{R}\right) e^{-\frac{R}{L}t}$$

where $R = R_s + R_D + R_0 + \Omega$

Therefore, the energy per cycle input to the coil is,

$$\frac{1}{2} L I_0^2 \left[\sin^2(\omega t - \phi) - 2\sin(\omega t - \phi)\sin(-\phi) e^{-\frac{R}{L}t} + \sin^2(-\phi) e^{-\frac{2R}{L}t} \right] \quad \text{where} \quad \phi = \tan^{-1}\frac{\omega L}{R}$$

for a complete steady state $t \rightarrow \infty$ and the above expression is,

$$\frac{1}{2} L I_0^2 \left[\sin^2(\omega t - \phi) \right]$$

This represents the maximum magnetic energy input to the coil. The ratio of the Maximum to transient energy is,

$$\text{Ratio} = 1 - \frac{2 \sin(-\phi)}{\sin(\omega t - \phi)} e^{-\frac{R}{L} t} + \frac{\sin^2(-\phi)}{\sin^2(\omega t - \phi)} e^{-\frac{2R}{L} t}$$

for $\omega = 2\pi f = 1/T$ and $t = T$, this reduces to,

$$\text{Ratio} = 1 - 2 e^{-R/Lf} + e^{-2R/Lf}$$

If it is assumed that the induced resistance of the core is proportional to the magnetic energy to the coil, the ratio expression represents the fraction of induced resistance for the core due to the lack of a full sinusoidal steady state being established.

A plot of this expression for the experimental circuit is shown in Figure (21). Note that at

$f = 0$, Ratio = 1.0

$f = \infty$, Ratio = 0

Thus for short transient periods, only a small fraction of the maximum energy is input to the coil.

Appendix A derives the expression for the total coil-core resistance as,

$$R_L = \Omega \left[1 + \frac{Q}{\pi} \right]$$

NO. 340-L21 DIETZGEN GRAPH PAPER
LOGARITHMIC
2 CYCLES X 1 CYCLE

EUGENE DIETZGEN CO.
MADE IN U. S. A.

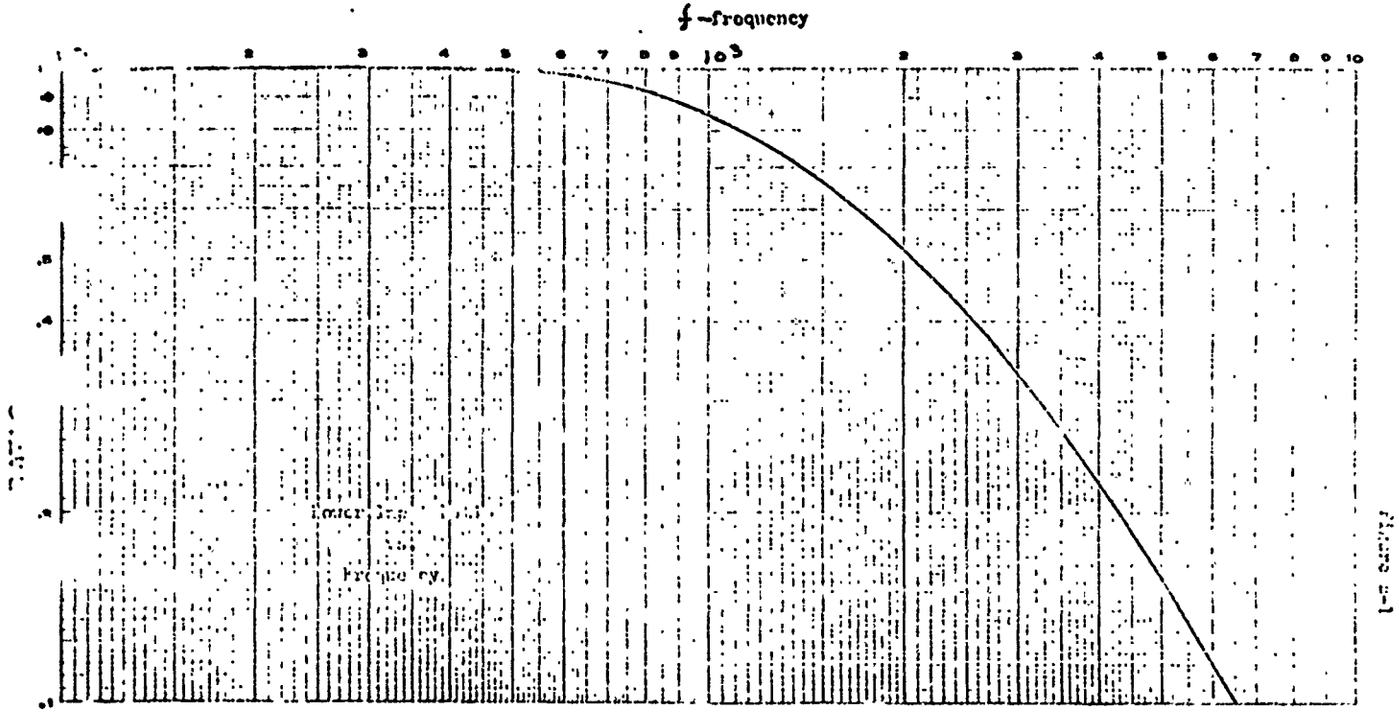

$\Omega_1 = \Omega_2 = 9.0$

$R_0 = 1.5$

$R_s = 4.0$

$R_p = 0$

The term $\frac{\Omega^2}{4}$ is proportional to the magnetic energy input into the coil. Thus, if it is reduced by the ratio term, some measure of the effect of the non-sinusoidal steady state on the theoretical results can be obtained. This effect on R_L is shown in Figure (E2), for the present bridge circuit. Note that the effect is one of importance primarily at high frequencies.

Other parameters could also reduce the theoretical value of the induced resistance. Amongst these are: mutual inductance between coils, contact resistances, and effects of the core fields.

An accounting for this can be made by including another reduction factor, C, into the expression for R_L. Thus,

$$R_L = \Omega\left[1 + \frac{\Omega^2}{4} \cdot \text{RATIO} \cdot C\right]$$

This factor can be determined experimentally and used as a correlating factor for the particular bridge circuit.

It should be noted that the application of the ratio factor is but an approximation and should be viewed as such. For a rigorous derivation of the non-sinusoidal effect, Maxwell's equations should be solved with the non-sinusoidal behavior of the input current. The difficulty of carrying out such an analysis is beyond the purpose of the project. Therefore, the ratio factor serves as an approximation to the true behavior of the circuit.

Figure B-2

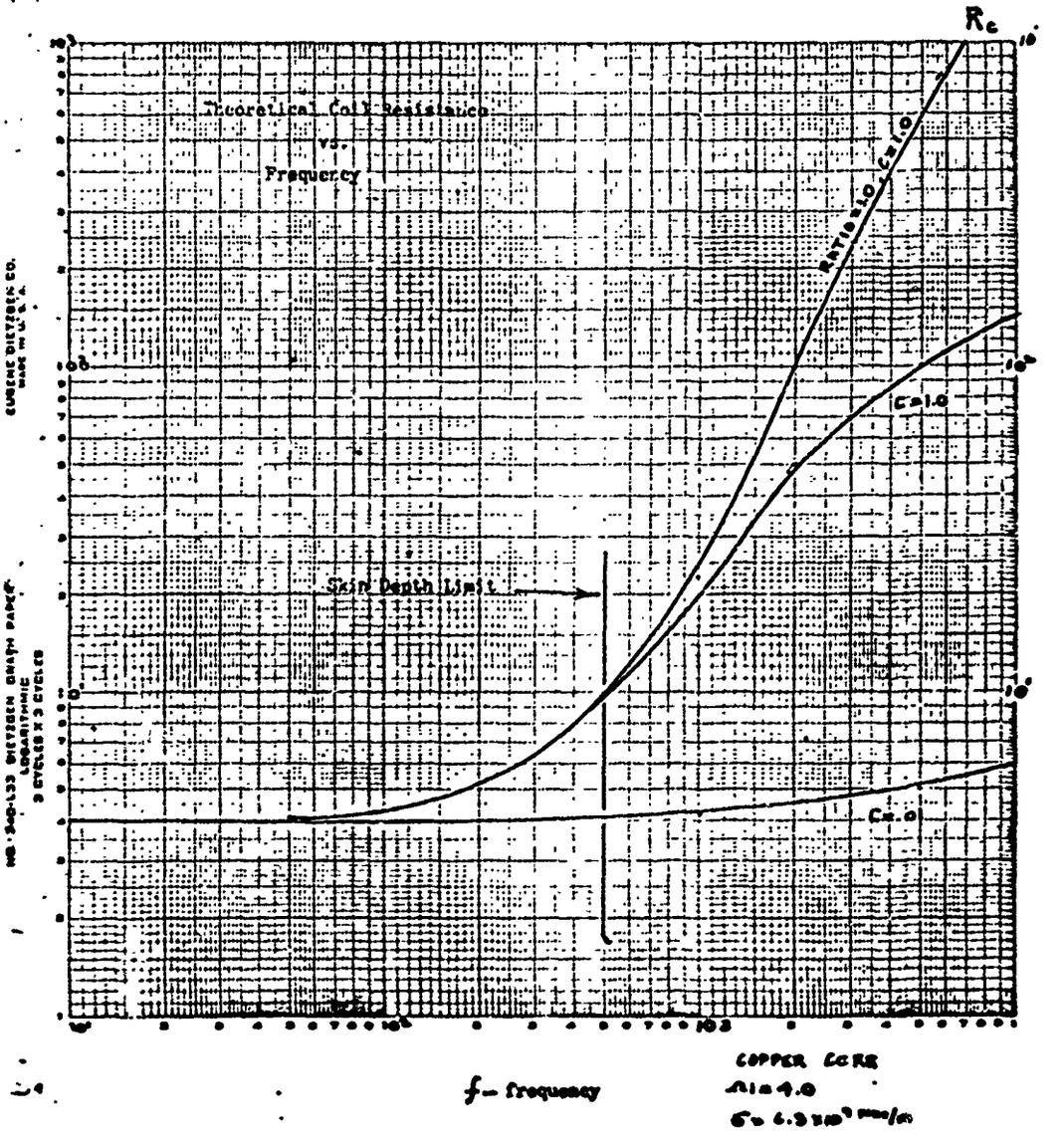
Theoretical Coil Resistance
vs.
Frequency
R_c
Ratio = 1.0, C = 1.0
C = 1.0
C = 0
Skin Depth Limit
f – frequency
COPPER CORE
$\mu_1 = 4.0$
$\sigma = 6.3 \times 10^3$ mho/m

Appendix C

Experimental Data

	Frequency	Air E_c	Metal E_o	ΔE_o	
Aluminum	2000	.78	.78	0	
	1500	1.05	1.05	.02	sine wave
	1000	1.43	1.52	.09	E_i = 1.0.
	800	1.65	1.80	.15	R_o = 7.5
	600	1.90	2.10	.20	R_B = 0
	400	2.25	2.40	.15	
	250	2.75	2.90	.15	
Brass	250	2.70	2.80	.10	
	400	2.28	2.42	.14	
	600	1.85	2.0	.15	
	800	1.52	1.65	.13	
	1000	1.38	1.50	.12	
	1500	1.02	1.08	.06	
	2000	.78	.78	0	
Copper	2000	.78	.10	-.68	
	1500	1.03	.54	-.49	
	1000	1.45	1.25	-.20	
	800	1.70	1.65	-.05	
	600	2.	2.15	.15	
	400	2.3?	2.68	.38	
	300	2.65	3.05	.40	
	250	2.80	3.30	.50	
	200	3.20	3.50	.30	
		millivolts	millivolts	millivolts	

	frequency	Air E_o	Metal E_o	ΔE_o	
Aluminum	2000	.88	.85	.03	
	1500	1.18	1.22	.04	Sine wave
	1000	1.60	1.77	.17	$E_i = 1.0$
	800	1.88	2.05	.17	$R_o = 10.0$
	600	2.18	2.40	.22	$R_B = 0$
	400	2.50	2.70	.20	
	200	3.20	3.35	.15	
	150	2.75	2.60	.05	
Brass	200	2.60	2.70	.10	
	400	2.25	2.38	.13	
	600	2.05	2.25	.20	
	800	1.75	1.95	.20	
	1000	1.54	1.66	.12	
	1500	1.15	1.23	.08	
	2000	.90	.95	.05	
Copper	1500	1.20	.65	-.55	
	1000	1.55	1.40	-.05	
	800	1.80	1.85	.05	
	600	2.15	2.40	.15	
	400	2.40	2.85	.45	
	250	2.90	3.30	.40	
	200	3.20	3.50	.30	
		millivolts	millivolts	millivolts	

	frequency	Air E_o	Metal E_o	ΔE_o	
Aluminum	250	.35	.38	.03	Square wave
	300	.44	.48	.04	$E_i = 3.0$
	400	.60	.62	.02	$R_o = .10$
	300	.56	.58	.02	$R_B \neq 0$
	500	.54	.555	.015	
	600	.49	.510	.02	
	700	.44	.45	.01	
	800	.40	.41	.01	
	900	.32	.37	.01	
	1000	.335	.335	0	
	1250	.255	.260	.05	
	1500	.205	.210	.05	
	2000	.140	.140	0	
	250	1.50	1.65	.05	$R_o = .50$
	300	1.72	1.76	.04	$E_i = 3.0$
	400	1.68	1.70	.06	$R_B \neq 0$
	500	1.56	1.60	.04	
	600	1.43	1.46	.03	
	700	1.29	1.31	.02	
	800	1.16	1.18	.02	
	900	1.0	1.03	.03	
	1000	.90	.92	.02	
	1250	.72	.74	.02	
		millivolts	millivolts	millivolts	

	frequency	Air E_0	Metal E_0	ΔE_0	
Brass	250	1.03	1.05	.02	Square wave
	300	1.01	1.04	.03	$E_1 = 3.0$
	400	.92	.94	.02	$R_e = .10$
	500	.715	.73	.015	$R_s = 0$
	600	.625	.640	.015	
	800	.465	.48	.015	
	1000	.370	.390	.010	
	1500	.225	.230	.005	
	2000	.155	.155	0	
Aluminum	2000	.155	.150	.005	
	1500	.225	.230	.005	
	1000	.370	.380	.010	
	800	.465	.475	.010	
	600	.60	.615	.015	
	500	.690	.705	.015	
	300	.970	.990	.020	
	200	1.0	1.01	.01	
Copper	250	.99	1.02	.03	
	300	.96	1.00	.04	
	400	.87	.90	.03	
	500	.77	.78	.01	
	600	.67	.66	.01	
	800	.515	.475	.06	
	1000	.41	.34	.07	
		millivolts	millivolts	millivolts	

APPENDIX D

COMPUTER PROGRAM

PROGRAM FOR CALCULATION OF T BRIDGE VOLTAGE OUTPUT

```
C       B T LUBIN  NONLINEAR T BRIDGE VOLTAGE OUTPUTCALCULATION
        DIMENSION RO(100), SIG1 (100), SIG2 (100),     F(500), E(50
        READ 2, J, L, M
    2   FORMAT( 3I3  )
        READ 4 , ( RO(K) , K= 1, J )
    4   FORMAT ( 6E10.3  )
        READ 4, ( SIG1(I) , I = 1, L )
        READ 4, ( SIG2 (II) , II= 1,M  )
        READ 4 , RS ,RD1,RD2,OMEG1,OMEG2,XL1,XL2,RADIUS,FMAX,RATIO
        PRINT 12, RS,RD1,RD2,OMEG1,OMEG2,XL1,XL2,RADIUS,FMAX,RATIO
   12   FORMAT ( 20H T BRIDGE OUTPUT                                //
     1 13H INPUT DATA  ,/
     2 2X,8H RS=     E10.3,2X,8H RD1=    E10.3,2X,8H RD2=     E10.3
     3 2X,8H OMEG1= E10.3,2X,8H OMEG2= E10.3, 2X,8H L1=    E10.3,
     4 2X,8H L2=    E10.3,2X,8H RADIUS=E10.3,2X,8H FMAX=   E10.3,
     5 2X,8H RATIO= E10.3          // )
        DO 4000 K = 1, J
        DO 3000 I = 1, L
        DO 2000  II = 1, M
        PRINT 14 , RO(K) , SIG1( I ) , SIG2 (II)
   14   FORMAT ( / 18H OUTPUT RESISTOR =    E10.3, 7H COND1=  E10.3
     1  7H COND2=   E10.3            // )
        PRINT 16
   16   FORMAT ( 20H OUTPUT CALCULATIONS                          /
     1 1X, 10H FREQUENCY,2X,10H EOUT/EIN  ,2X, 10H RCORE1      ,2X
     2 10H RCORE2          ,2X, 10H RESIST1  ,2X, 10H RESIST2  ,
     3 2X, 10H RATIO              /  )
C       START OF CALCULATIONS
        RAD = RADIUS * .0254
        XMU = .00000126
        F(1 ) = 1.0
        PI = 3.14
        DELT = 1.0
        E(0 ) = 0.0
        DO 1800 N = 1, 500
        XR = RS + RD1 + RO(K) + OMEG1
        Z = XR/ (XL1 * F(N)  )
        XRATIO = RATIO*(1.   -2.*EXPF(-Z) + 1. *EXPF(-2.*Z) )
        A = ( XMU * RAD **2 * ( 2. * PI ) **2/8. ) * XRATIO
        RC1 = OMEG1* ( 1.+A*SIG1(I) * XL1*F(N) **2 / OMEG1)
        RC2= OMEG2* (1.+ A*SIG2(II) *XL2 *F(N) **2 / OMEG2 )
        R1 = RS + RD1 + RO(K) + RC1
        R2 = RS + RD2 + RO(K) + RC2
        R = ( R2 - R1 ) / ( R1 * R2 )
        XK1 = R1 / ( 2. * XL1 * F(N)  )
        XK2 = R2 / ( 2. * XL2 * F(N)  )
        XXK1 = ( 1. / XK1 ) * ( EXPF(-XK1 ) - 1.0      )
        XXK3 = XXK1 / R1
        XXK2 = ( 1. / XK2 ) * ( EXPF(-XK2 ) - 1.0      )
        XXK4 = XXK2 / R2
        EOEI = ( RO(K) / 2. ) * ( R + XXK3 - XXK4  )
        E(N) = EOEI
C       PRINTING OF OUTPUT
        PRINT 18, F(N), E(N), RC1, RC2, R1, R2, XRATIO
```

```
   18   FORMAT ( 7E12.5 )
C       FREQUENCY CYCLE CALCULATION
        IF ( F(N) - FMAX ) 100 , 100, 2000
  100   F(N+1 ) = F(N)  + DELT
        IF ( F(N+1 ) / DELT - DFCT )  1800, 1800, 120
  120   F(N) = 0.0
        DELT = 10. * DELT
        F( N + 1 ) = F(N) + DELT
 1800    CONTINUE
 2000   CONTINUE
 3000   CONTINUE
 4000   CONTINUE
        CALL EXIT
        END
```